

Chapter 1

Vapor–Liquid–Solid Growth of Semiconductor Nanowires

Heon-Jin Choi

Abstract Nanowires make possible to manipulate light in novel methods and thus are promising materials for advanced optoelectronics. To exploit the potential, the growth behavior has to be controlled since it dominates the physical and chemical states and, in turn, the optical properties of nanowires. In this chapter, the vapor–liquid–solid (VLS) mechanism for the growth and modulation of nanowires was discussed. The chapter first reviewed the fundamental aspects of the VLS mechanism. Then the state of the art of the growth and modulation of nanowires for optoelectronics were discussed from the point of view of the critical issues pertaining to this mechanism. Some examples of optoelectronic devices that had been fabricated based on the VLS mechanism were also reviewed in an effort to cover the cutting edge technology in this area. Lastly, a summary and several different perspectives on the VLS mechanism were presented.

1.1 Introduction

Nanowires are hair-like, one-dimensional (1D) nanomaterials with diameters in the sub-one hundred nanometer scale and lengths ranging from several hundreds of nm to as high as a few cm. Owing to their nanoscale dimensions in the radial direction, they have size confinement effects that give them novel physical properties as compared to bulk materials. Their one-dimensional geometry on the nanometer scale provides an extremely high surface area with a nanoscale radius of curvature and great mechanical flexibility with near theoretical strength. These properties are advantageous in many chemical and mechanical applications. The geometry also

H.-J. Choi (✉)

Department of Materials Science and Engineering, Yonsei University, 50 Yonsei-ro, Seodaemun-gu, Seoul 120-749, Korea

e-mail: hjc@yonsei.ac.kr

provides anisotropic properties that should be interesting from the point of view of nanomaterials science and engineering. Their length, reaching as high as the cm scale, makes them easy to manipulate for device fabrication.

Nanowires are promising materials for advanced optoelectronics. In addition to the unique aspects of their physical, chemical, and mechanical properties, the size of these materials is comparable to visible light in wavelength from 400 to 650 nm. This implies that nanowires can be used to handle light on a nanometer scale and thus can be used as building blocks for advanced optoelectronics. Indeed, novel methods of the manipulation of light with nanowires, including nanoscale Fabry–Perrot mode stimulated emission, wave guiding of photons, random lasing action, highly efficient luminescence, and extremely sensitive photodetection, have recently been demonstrated. The concept of many advanced nanowire-based optoelectronic devices including light-emitting diodes (LEDs), lasers, optical sensors, photo diodes, and photovoltaic cells have also been demonstrated.

The physical and chemical states of nanowires dominate their optical properties. The length and diameter of nanowires as well as their alignment affect the emission and absorption properties. The composition, impurity, or doping level, defect concentration, crystal structure, growth direction, and nature of the facets are also critical to the emission and/or stimulated emission and absorption. It should be noted that these physical and chemical states are closely related to the growth of nanowires. Therefore, one must fully understand the growth behavior of nanowires and develop rational, reliable growth processes to exploit the potential of nanowires in optoelectronics.

Nanowires are a result of anisotropic, 1D crystal growth on a nanometer scale. Therefore, the key issue related to the growth of nanowires is how to induce 1D crystal growth in a controlled manner. Regarding this, many approaches have been studied, including the use of the metal-catalyst-assisted vapor–liquid–solid (VLS) mechanism, the vapor–solid (VS) mechanism, and the template-assisted (TA) mechanism. Among these, the VLS mechanism is the most widely used owing to its simplicity and versatility when applied in many semiconductor systems.

This chapter reviews the growth of semiconductor nanowires by the VLS mechanism in the area of optoelectronics. As mentioned earlier, the growth process is critical to the physical and chemical state of nanowires and thus their optical properties. Therefore, a review of the growth process may be helpful so as to facilitate the preparation of superior nanowires for optoelectronics. This chapter focuses on the VLS mechanism. This may, however, limit our viewpoint regarding the growth of nanowires, as other mechanisms are also available. However, the VLS mechanism is a mainstay at present. Therefore, it may be sufficient to review the state of the art of this area. This chapter seeks to explain the understanding of what the VLS mechanism is as well as the manner in which better nanowires can be grown for optoelectronics. Accordingly, the chapter first reviews the fundamental aspects of the VLS mechanism. The growth of nanowires and a number of critical issues pertaining to VLS mechanism follow. Some examples of optoelectronic devices that have been fabricated based on the VLS mechanism are also reviewed in an effort

to cover the cutting edge technology in this area. Lastly, a summary and several different perspectives on the VLS mechanism are presented.

1.2 VLS Mechanism for One-Dimensional Crystal Growth

The VLS mechanism is a 1D crystal growth mechanism that is assisted by a metal catalyst. It results in the creation of whiskers, rods, and wires. 1D crystal growth was initially developed nearly 50 years ago in the Si industry and the mechanism was suggested for wider use by Wagner in 1964 [1]. Figure 1.1 shows a schematic of the VLS mechanism. In this mechanism, the metal catalyst forms liquid alloy droplets at a high temperature by adsorbing vapor components. For some reason, e.g., temperature or vapor pressure fluctuation, the alloy is further supersaturated; i.e., it becomes a solution in which the actual concentration of the components is higher than the equilibrium concentration. It then drives the precipitation of the component at the liquid–solid interface to achieve minimum free energy of the alloy system. Accordingly, the 1D crystal growth begins, and it continues as long as the vapor components are supplied. Because vapor (carries solid components), liquid (catalyst alloy), and solid (precipitated one-dimensional structures) phases are involved, it is known as the VLS mechanism. At a glance, one can know that the size and position of the catalyst are related to the diameter and position of the 1D structures, as the liquid phase is confined to the area of the precipitated solid phase.

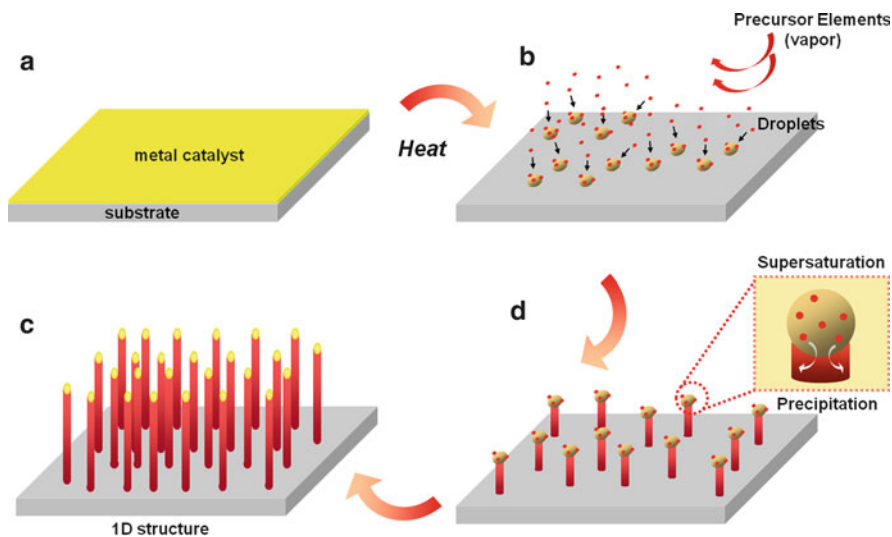


Fig. 1.1 Growth of 1D structures by VLS mechanism

The mechanism works at a high temperature at which the metal catalyst forms a liquid alloy. Therefore, chemical processes that occur at high temperatures, such as chemical vapor deposition (CVD), molecular beam epitaxy (MBE), laser ablation (LA) and carbothermal reduction (CR), are generally used in conjunction with the mechanism. Occasionally, metal catalysts sometimes work in a solid state in a vapor or liquid phase environment in a process termed the VSS (vapor–solid–solid) or LSS (liquid–solid–solid) mechanism.

Since the 1970s, the mechanism has been used to grow various types of whiskers on the micrometer or mm scale. A typical example is SiC whiskers, which are excellent reinforcements for high-strength, high-toughness ceramic or metal composites [2]. In this application, larger whiskers have a better reinforcing effect; thus, the catalyst size is made to be as large as possible, up to more than 10 μm , to grow large-diameter SiC whiskers, as shown in Fig. 1.2.

The mechanism was then noted for the growth of 1D structures on a nanometer scale, i.e., nanowires, in the 1990s, and the feasibility of this was demonstrated by several groups, including the Lieber group at Harvard University, the Yang group at the University of California Berkeley, and the Samuelson group at Lund University. As this mechanism was slated to become a core method for the growth of semiconductor nanowires, unambiguous experimental evidence of this mechanism was required for further study. Regarding this, Yu directly observed the growth of Ge nanowires by using an in situ high-temperature transmission electron microscope [3]. The findings of Yu's study showed that there are three well-defined stages in the VLS mechanism: alloying (note that the catalyst in Fig. 1.3a–c becomes larger as the Ge component dissolves and becomes alloyed with Au), precipitation of Ge (the bright area in c and d), and axial growth (extended structures in e and f).

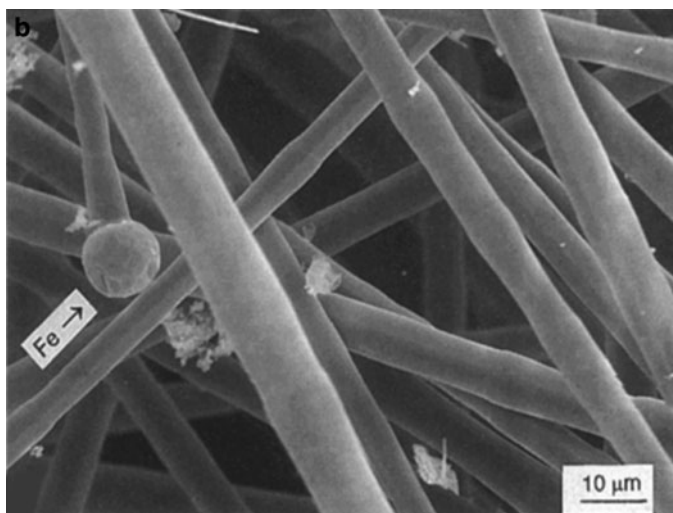
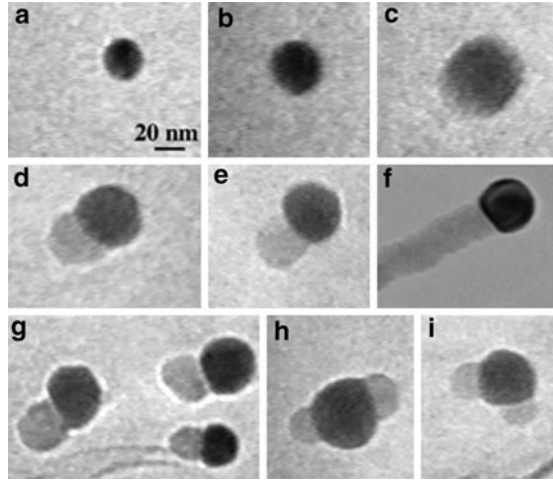


Fig. 1.2 SiC whiskers grown by VLS mechanism using Fe as catalyst (after [2])

Fig. 1.3 Direct observation of growth of 1D Ge structures by VLS mechanism using Au as catalyst (after [3])



This observation clearly supports the proposed VLS mechanism, which is shown in Fig. 1.1. Other observations regarding the growth of Si nanowires on the substrate further confirmed the working of the VLS mechanism with the assistance of a liquid catalyst [4].

The brief history of the VLS mechanism implies that it can be generally used for the growth of many 1D structures, from the nm to even the mm scale. It also shows the rising of new technology from old technology as a good example of the progress of science and technology from previous studies. In fact, previous studies have established some fundamental aspects, as discussed below, which are essential for growing 1D structures using a catalyst.

1.2.1 Requirements for Metal Catalyst

Metal catalysts are essential in the VLS mechanism, but not all metals can work. These meet the following requirements: (1) It must form a liquid solution with a component of the solid phase. (2) The solubility limit of the catalyst component in the liquid phase must be much higher than that in the solid phase (i.e., $K = C_s/C_l < 1$, where C_s is the solubility limit in the solid phase and C_l is the solubility limit in the liquid phase). Under this condition, the catalyst easily leads to the formulation of the liquid alloy with little contamination in the solid phase. (3) The vapor pressure (V_p) of the catalyst component over the liquid alloy should be small. Otherwise, the catalyst will evaporate and eventually disappear in the course of growth. (4) It must be inert to chemical reactions. Otherwise, a reaction could deprive it of its catalytic function. (5) It must not make an intermediate solid. Otherwise, the intermediate solid will also deprive it of its catalytic function [1].

Previous studies have revealed that some metals meet the requirements. Generally, noble and transition metals work well with the VLS mechanism. For example,

Au works well for the growth of a 1D structure of group IV materials (e.g., Si and Ge), oxides (e.g., ZnO), and III–V semiconductors. Transition metal such as Ni and Fe also work for the growth of group IV materials (e.g., Si, Ge, and SiC) and III–V semiconductors. Naturally, many studies have focused on these metals to grow 1D structures. However, it should be noted that many other metals can also be developed as a catalyst for the VLS mechanism [5].

1.2.2 Phase Diagram

Because the adsorption, dissolving, mixing, diffusion, and precipitation in the liquid phase are thermodynamic processes that work toward equilibrium, a phase diagram is useful to predict how a catalyst will work. Figure 1.4 shows the phase diagram of the Au–Si system, which can be referred to regarding the growth of 1D Si structures with Au [6]. The diagram indicates that the minimum growth temperature for Si should be higher than the eutectic point of the system (364°C). The diagram also indicates that the composition of the Au–Si alloy above the eutectic point will follow the liquidus line (solid line) that denotes equilibrium between the solid and liquid phase. Therefore, the composition of the liquid alloy can be found at the liquidus line (point A) at a given temperature (1,100°C in the diagram). However, some temperature or vapor pressure fluctuation over the liquid alloy dissolves more Si

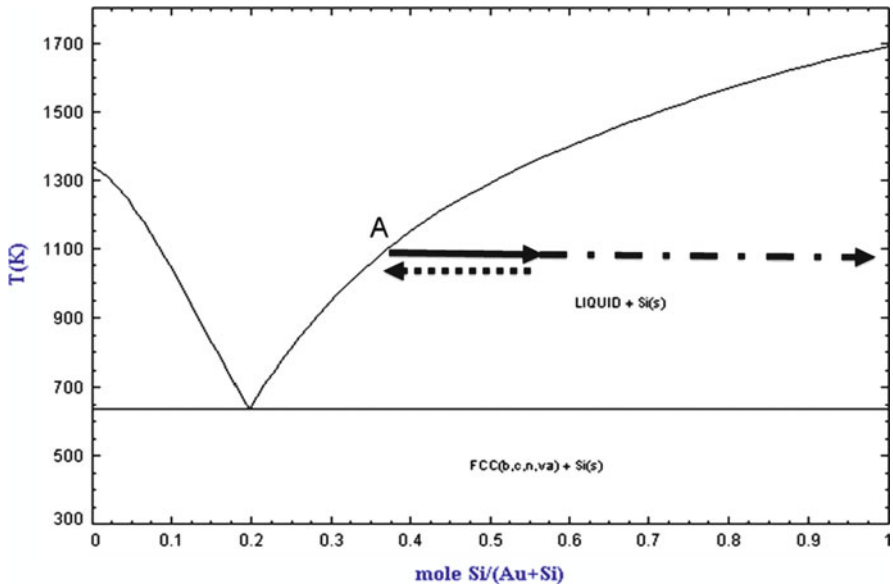


Fig. 1.4 Phase diagram of Au–Si system with indication of the composition of liquid alloy catalyst in the course of growth of 1D structures by VLS mechanism

than the equilibrium composition and renders it into a supersaturated state. As a result, the composition of the alloy goes beyond the equilibrium composition, moving to the right side of the liquidus line (solid arrow). This supersaturation state is thermodynamically a nonequilibrium and unstable state and thus drives the precipitation of the solid phase from the supersaturated liquid alloy until an equilibrium state is reached. The composition will then move back to the left and reach the liquidus line (dashed arrow). The composition of the precipitated solid phase corresponds to that of the phase boundary and thus is pure Si according to the diagram (dashed dot arrow). Meanwhile, the composition of the alloy goes beyond the equilibrium composition again as Si is dissolved from the vapor and drives the additional growth of 1D structures with the precipitation at the interfaces.

It should be noted that the currently available phase diagrams are constructed from bulk systems. Because the thermodynamic properties of a nanosystem are wholly different from those of a bulk system, the phase diagram of the type of nanometal catalyst that we are interested in should differ from that of the bulk system. Indeed, Eli and Peter Sutter investigated the equilibrium composition of nanoscale Au–Ge alloy droplets at the tips of Ge nanowires and found that the equilibrium composition of these droplets deviates significantly from that of the bulk alloy (Fig. 1.5) [7]. Adhikari et al. also investigated Au-catalyzed Ge nanowire and constructed a binary Au–Ge phase diagram that shows the catalyst size-dependent liquidus temperature [8]. These phenomena may be due to the critical role of the surface energy in the nanosystem [7–10]. Regardless of the cause of the deviation, it should be considered that the different thermodynamic equilibrium of the nanosystem causes discrepancies between the actual growth behavior of nanowires through a nanometal catalyst and predictions on the basis of a diagram of the bulk system.

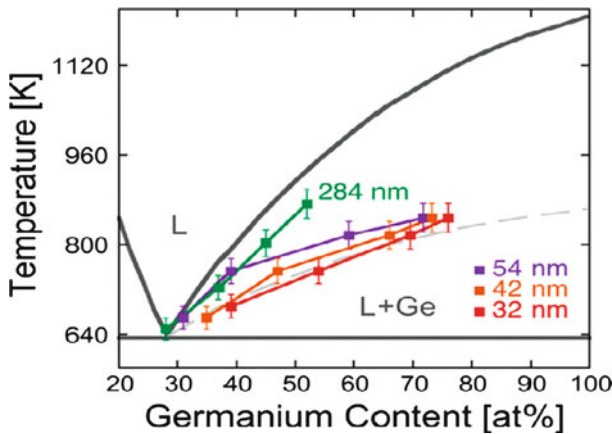


Fig. 1.5 Au–Ge binary alloy phase diagram. The *solid gray curves* represent the Au and Ge liquidus and solidus lines, respectively. *Squares* represent measurements of the temperature-dependent Ge content of Au–Ge alloy drops at the tip of Ge nanowires (after [7])

1.2.3 Kinetics and Rate-Determining Step

Three phases (gas, liquid, and solid) and two interfaces (gas/solid and liquid/solid) are involved in the VLS mechanism. In these complex system, the kinetics of the VLS mechanism consists of four steps: (1) mass transport in the gas phase; (2) chemical reaction at the vapor–liquid interface; (3) diffusion in the liquid phase; and (4) incorporation of atoms in a crystal lattice (Fig. 1.6) [11–14]. Identification of the rate-determining step among these is important to control the overall kinetics of the VLS mechanism. However, this is complicated, as three phases, two interfaces, and chemical reactions are involved [11]. Nevertheless, it may be possible to draw some insight based on the experimental results. As an example, the rate-determining step for the growth of 1D Si structures with an Au catalyst could be postulated as follows: Among the steps, step (3) can be excluded, because atoms diffuse in liquid metals very quickly [12] and thick nanowires or whiskers do not grow more slowly than those that are thinner, while the shape of the liquid droplet is maintained as nearly hemispherical and thus retains a longer diffusion length [11]. Step (1) can also be excluded because the diffusion coefficient in the gaseous phase usually follows the following power law: $D = D_0(T/T_0)^n(P/P_0)$, $n = 1.5 \sim 2$ [11, 12]. Therefore, the growth rate should follow the power law. However, this is not the case in many cases [11–14]. The primary evidence for regarding step (2) as the rate-limiting step is that the growth rate is proportional to the partial pressure of the reactant gas. However, this does not fully support the argument given that the growth process consists of two activated steps in series [11]. The dependence of the growth rate on the reactant vapor concentration is not in itself evidence that any of the steps is the rate-determining step. Rather, it simply reflects the dependence of the growth rate on supersaturation. Therefore, the rate-determining step would be step (4), the incorporation of atoms in a crystal lattice. It should be noted that the rate-determining step can be changed by the materials involved in the kinetics and by the processing conditions. Therefore, it should be carefully postulated by

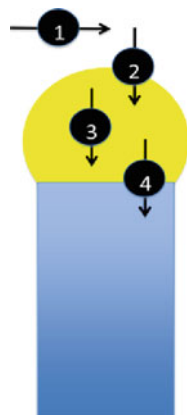


Fig. 1.6 Kinetic steps in VLS mechanism: (1) mass transport in the gas phase; (2) chemical reaction on the vapor–liquid interface; (3) diffusion in the liquid phase; and (4) incorporation of atoms in a crystal lattice

as many experimental results and data as possible. In fact, the postulation here is possible because a considerable amount of experimental data regarding the growth of Si whiskers, rods, and recently nanowires is available in the literature.

1.2.4 Size of the Metal Catalyst

As described earlier, nanowires can be grown using a nanometer-sized metal catalyst because the diameter of a 1D structure is confined by the size of the catalyst. Indeed, the bulk of previous studies demonstrated the growth of nanowires using nanofilms (that convert to nanoliquid droplets at a high temperature due to surface tension) or nanoparticles. However, it is difficult to decrease the size of the catalyst and in turn the diameter of nanowires in an unlimited manner. Thermodynamically, the minimum radius of a liquid metal droplet is given as [15]

$$R_m = \frac{2V_l}{RT \ln(s)} \sigma_{lv}, \quad (1.1)$$

where V_l is the molar volume of the droplet, σ_{lv} is the liquid–vapor surface energy, and s is the degree of supersaturation of the vapor. According to this equation, using a smaller catalyst requires a higher degree of supersaturation. However, the chemical potential of the component in the metal–alloy catalyst becomes high as the size of the catalyst decreases due to the Gibbs–Thompson effect:

$$\Delta\mu = \frac{2\gamma}{r}. \quad (1.2)$$

Here, $\Delta\mu$ is the chemical potential difference of the component species in the liquid droplet, γ is the surface energy, and r is the radius of curvature of the droplet. Therefore, dissolving a vapor component into a liquid alloy becomes increasingly difficult as the size decreases, making it difficult to reach supersaturation states that sufficiently induce the growth of nanowires. Indeed, it is known that the growth of 1D structures with diameters of several tenths of nm is feasible; however, ensuring a smaller diameter (e.g., sub-10 nm) is difficult due to the thermodynamic limitations associated with the use of a nanocatalyst.

An additional difficulty that arises when downsizing a catalyst comes from the manipulation of metal nanoparticles or droplets. It is well known that nanoparticles have strong van der Waals attractive forces and thus agglomerate into larger particles. Furthermore, Ostwald ripening occurs between nanoparticles at high temperature. Ostwald ripening is a spontaneous process that occurs because larger particles are more energetically favorable. Accordingly, nanoparticles tend to transform into large particles to attain a lower energy state if the temperature is high enough to induce diffusion of the metal component. Because the van der Waals attractive forces and Ostwald ripening lead to the formation of larger droplets, larger diameter 1D structures are often grown from a nanometal catalyst. Thus, metal nanoparticles

have to be carefully separated from each other in the course of the preparation, positioning on the substrate, and heating for the growth of 1D structures.

1.3 Growth of Nanowires by the VLS Mechanism and Current Issues for Optoelectronics

1.3.1 Growth of Semiconductor Nanowires by the VLS Mechanism

Si nanowires are a typical case of the growth of nanowires by the VLS mechanism with the assistance of a metal catalyst. Typically, Si nanowires are grown by Au because this metal meets the requirements for a VLS catalyst. The eutectic point of the Au–Si system is low, the phase relationship is simple and the system is stable at high temperatures. Figure 1.7 shows Si nanowires grown by the VLS mechanism using Au as a catalyst and SiCl_4 as the Si precursor [16]. The SEM images shown in Fig. 1.7a reveal Si nanowires with diameters of ~ 100 nm and lengths of several μm that were grown on a Si substrate coated with Au film with a thickness of 2 nm. It also shows that the nanowires grew vertically on the substrate. It is well known that an epitaxial relationship between the substrate and nanowires can be attributed to the vertical growth of nanowires [17]; thus, the vertical growth here indicates that Au yields epitaxial interfaces between the nanowires and Si substrate. The transmission electron microscopy (TEM) images and selected area electron diffraction (SAED) patterns in Fig. 1.7b clearly show that the Si nanowires are single-crystalline nanowires without any structural defects. Alloy globules of Au–Si formed at the tips of the nanowires. An energy-dispersive spectroscopy (EDS) analysis across the catalyst–nanowire interface at the tip of an individual nanowire shows that Au operates as a VLS catalyst in this case. Note that an Au-rich globule formed when the Au catalyst was used according to the phase diagram of the Au–Si binary system (Fig. 1.4). Characterization of the catalyst globule/nanowire interfaces by high-resolution transmission electron microscopy (HRTEM) reveals

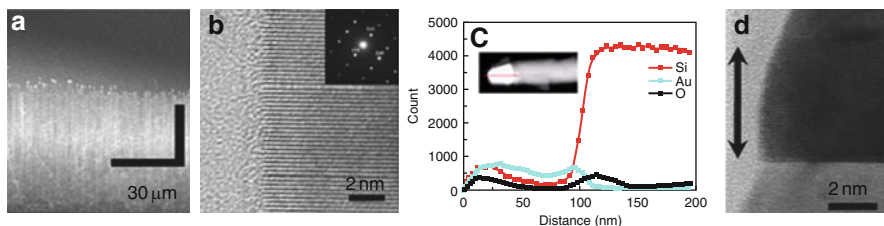


Fig. 1.7 Si nanowires grown by VLS mechanism using Au as catalyst. The nanowires were grown in the [110] direction for (110) Si substrates. (a) SEM image of Si nanowires, (b) TEM image and diffraction pattern, (c) EDS analysis of catalyst, (d) HRTEM image of the interface (after [16])

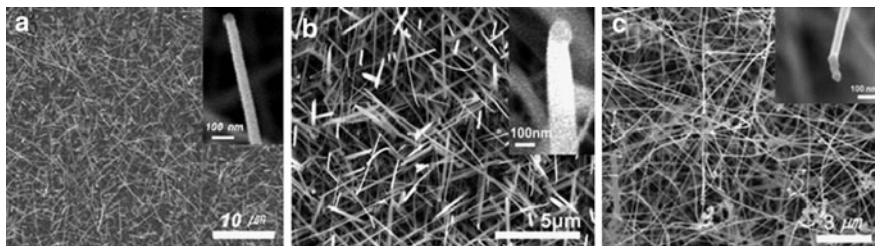


Fig. 1.8 (a) Ge, (b) GaN, and (c) ZnO nanowires grown by VLS mechanism using metal catalyst of Au, Ni, and Au, respectively. All these nanowires are single crystal

sharp interfaces between Si and catalyst (Fig. 1.7d). This indicates that there were no intermediate compounds. Taken as a whole, these outcomes indicate that Au is ideal catalyst that satisfies the requirements of a VLS catalyst.

Other semiconductor nanowires can also be grown by the VLS mechanism. Figure 1.8 shows Ge, GaN, and ZnO nanowires grown by the VLS mechanism using Au or Ni. The diameter and length of these nanowires typically range from 50 to 100 nm and tens of micrometers, respectively, depending on the size of the catalyst and the growth time. An HRTEM image of these nanowires indicates that they are single-crystalline in nature without defects or secondary phases. In fact, most nanowires grown by the VLS mechanism are of a single-crystal nature. These nanowires typically grow in the direction corresponding to the closest packing plane; however, this depends on factors such as the diameter of nanowires, the substrate used, the catalyst, and the processing conditions.

1.3.2 *Issues Associated with the VLS Mechanism for Optoelectronics*

As shown above, semiconductor nanowires can be grown by the VLS mechanism. However, some issues have to be addressed before the potential of nanowires can be exploited in the area of optoelectronics. By considering the nature of the VLS mechanism in conjunction with the findings of previous studies, these issues can be summarized as metal catalyst and structural modulation including control of the diameter, vertical growth, creation of coaxial and/or longitudinal heterostructure nanowire (COHN or LOHN), and compositional modulation including the alloying and doping of nanowires.

1.3.2.1 **Metal Catalyst**

Many metals are successfully used as VLS catalysts for the growth of nanowires. While they have important advantages for the controlled growth of nanowires, there

are some issues from the point of view of semiconductor engineering. For example, Au as a catalyst is used for the growth of many nanowires, including Si, Ge, ZnO, GaN, and GaAs. However, it inevitably becomes contaminated into the nanowires as a result of contact between the liquid Au alloy and the semiconductor at a high temperature [18]. This contamination can increase the impurity level in the band gap and thus degrade the optical properties of nanowires. Furthermore, Au is not compatible with current CMOS processes and thus is limited in terms of how it can be introduced into the CMOS process. The very high diffusivity of Au induces migration of this metal on the surface of Si nanowires, making it difficult to control the growth precisely [19]. Accordingly, efforts to find a suitable catalyst that will not degrade the optical properties of nanowires and that can be used in the CMOS process have been made.

For Si nanowires, Al is considered as a promising candidate because the Al–Si binary phase diagram is similar to that of Au–Si. Indeed, limited studies have shown the successful growth of Si nanowires using Al [20, 21]. For example, Ke et al. grew Si nanowires by thermal CVD using Al as the catalyst [20]. The Al, however, oxidized quickly, showing that a well-designed, airtight growth process is necessary. In their work, Ke et al. used high H_2 and SiH_4 partial pressures to suppress the Al oxidation.

The other candidate for Si nanowires is Pt. Pt is a noble metal and thus has similar physical properties to Au. Indeed, Pt also successfully works as a catalyst for the growth of Si nanowires [16]. Figure 1.9 shows scanning electron microscopy (SEM) images and TEM images of Si nanowires grown using Pt as a catalyst. The size of the Si nanowires is comparable to that of nanowires grown by Au. In this case, they

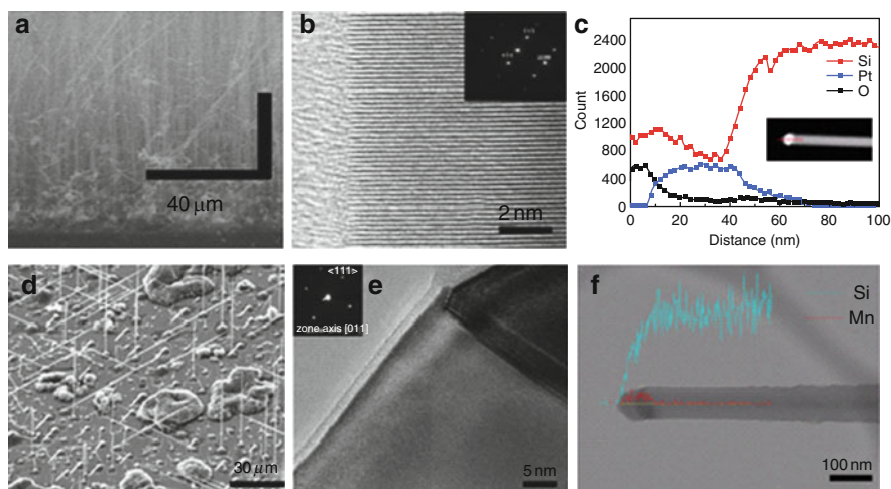


Fig. 1.9 Si nanowires grown by VLS mechanism with Pt (**a**, **b**, **c**) (after [16]) and Mn catalyst (**d**, **e**, **f**). (**a**), (**d**) SEM images of Si nanowires, (**b**), (**e**) TEM images of Si nanowires, (**c**), (**f**) EDS analysts of catalyst

grew vertically on the substrate. Hence, Pt yields an epitaxial interface between the nanowires and the Si substrate. It appears that the growth rate is generally faster than it is with Au under the same conditions. The Si nanowires are single-crystalline structures without any structural defects. Alloy globules of Pt–Si form at the tips of the nanowires. An EDS analysis across the catalyst–nanowire interface at the tip of an individual nanowire clearly shows that the Pt operated as a VLS catalyst, similar to Au.

Transition metals can also be considered as the VLS catalyst for the Si nanowires. For example, Mn can be used to grow Si nanowires. As shown in Fig. 1.9, the Si nanowires grown with Mn as a catalyst are tens of μm in length and tens of nm in diameter. Compared to other metal catalysts, such as Au or Pt [16], Mn catalysts lead to rather slow growth under the same growth conditions. The nanowires also have metal globules at their tips and, as shown in Fig. 1.9, consist of a Si–Mn alloy containing about 64% Si and 36% Mn. These globules clearly indicate that the nanowires were grown by the VLS mechanism with the assistance of Mn. In addition, there is no Mn in the nanowire body. These results indicate that many other metals can also be explored to grow Si nanowires. In fact, Ag, Bi, Cd, Co, Cu, Dy, Fe, Ga, Gd, Mg, Ni, Os, Pb, Pd, Te, Ti, and Zn can be explored as VLS catalysts for Si nanowires, as summarized by Shimit et al. [5].

GaN and ZnO nanowires are typically grown using a transition metal such as Ni and Au, respectively. As mentioned earlier, these metal catalysts can also increase the impurity level in the band gap and thus degrade the optical properties of nanowires. However, the M (metal catalyst)–Ga–N or the M–Zn–O system is complex compared to M–Si system. Therefore, it is likely that the number of catalysts available for these nanowires is limited as compared to Si nanowires. While many catalysts should have been explored for GaN nanowires, successful growth has not been reported thus far. In the case of ZnO nanowires, Sn has been reported as a VLS catalyst [22].

With regard to the formation of the impurity level in the band gap [23], the self-catalytic VLS mechanism is interesting. This mechanism works with a liquid catalyst that is formed in an in situ mode. For example, it was found that InAs nanowires can be grown without a metal catalyst [24]. Closer investigation revealed that a liquid In catalyst which forms from the substrate leads the growth of nanowires. Vertically aligned InP nanowires were also grown without a metal catalyst. It was revealed that temperature and precursor ratio control induces indium droplets to form on the surface and act as nucleation sites for nanowire growth [25]. This self-catalytic VLS mechanism is not commonly used, but it has the potential to grow nanowires without contamination of the catalytic components in some semiconductor systems.

1.3.2.2 Structural Modulation

To realize novel optical properties and newly fabricated devices, structural modulation of nanowires, such as control of the diameter, alignment, and growth-position,

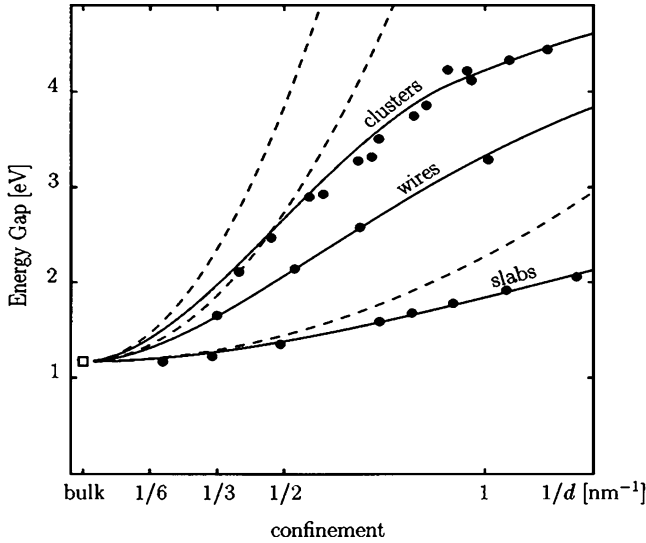


Fig. 1.10 Band-gap modulation of Si structures as a function of size (after [26])

is needed. Creating heterostructures in the radial or longitudinal direction is also crucial.

Diameter control: The optical properties of nanowires are dependent on their diameter. For example, the band gap, which determines the wavelength of luminescence, of semiconductor nanowires is renormalized by the diameter. Theoretical predictions of this type of band gap modulation are shown in Fig. 1.10, where the band gap of Si nanowires becomes wider as the diameter approaches the sub-10 nm scale [26]. Such small diameters also change the semiconductor characteristic of Si from an indirect to a direct band gap [27]. These findings imply that the optical properties of nanowires with both indirect and direct band gaps can be tuned by decreasing their diameter down to their Bohr exciton radius.

However, as described in Sect. 1.2, downsizing of the catalyst raises the chemical potential of the liquid alloy droplet and thus makes it difficult to grow nanowires with such a small diameter. This is thus a challenging issue from the point of view of thermodynamics. It should also be noted that these types of very thin nanowires have been grown using the VLS mechanism, though the optical properties in these cases have not been reported [28]. Therefore, these types of very thin nanowires can be grown for the development of indirect-band-gap nanowire-based optoelectronics.

With diameter control of direct-band-gap semiconductors such as GaN or ZnO, nanowires can also be created with novel optical properties such as multicolor luminescence by the quantum confinement effect. Indeed, such a novelty has already been demonstrated in GaN, InP and ZnO nanowires in which shifts in the emission spectra occur due to radial quantum confinement [29–31]. However, the growth of these nanowires reliably on the sub-10 nm scale using the VLS mechanism remains a challenging issue.

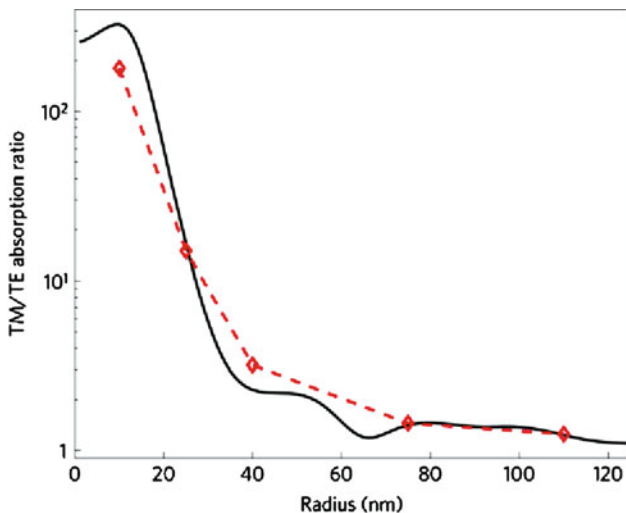


Fig. 1.11 Polarization dependence of the absorption efficiency, Q , and its dependence on Ge nanowire diameter. Theoretical calculations (*solid line*) and experimental measurements (*symbols*) on the ratio of the absorption efficiencies for transverse-magnetic- and transverse-electric-polarized 633 nm light (after [32])

Similar to the luminescence, the absorption of nanowires is dependent on the diameter. In a study of Ge nanowires [32], it was revealed that the absorption of nanowires is strongly dependent on the diameter, as shown in Fig. 1.11; due to the heavy transverse-magnetic/transverse-electric degeneracy in larger wires, the polarization dependence sharply drops as the diameter increases.

Vertical growth: A vertical array of nanowires provides novel optical properties that are advantageous for many applications, including nanolasers, LEDs, photovoltaic cells, and field emitters. For example, theoretical analysis indicates that vertical nanowire arrays have much lower reflectance compared to thin films. In a high-frequency regime, nanowire arrays have higher absorption than their thin film counterparts. In low-frequency regime, nanowire arrays absorb less but can be designed to approach the level of the film by changing the filling ratio [33]. Due to the low reflectance, it is possible to develop highly efficient photovoltaic devices. Other novel functions, such as direct conduction paths for photogenerated carriers, the creation of natural waveguiding cavities, and field emissions from arrayed atomicscale sharp tips can also be expected from the vertical nanowire array. The use of this type of array also enables the preparation of three-dimensional optoelectronic architectures.

The vertical growth of Si nanowires by the VLS mechanism is relatively easy, as many previous studies have demonstrated, as Si wafers are readily available as a substrate. Because the most rational approach to grow nanowire vertically is to establish an epitaxial relationship between the nanowire and the substrate,

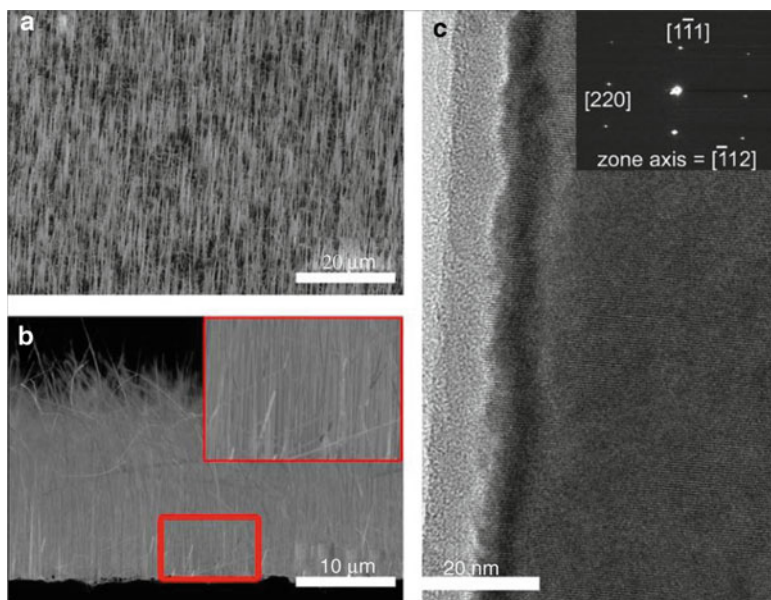


Fig. 1.12 SEM images of Mn:Ge nanowires vertically grown on Ge (111) substrate in a (a) 45°-tilted and (b) cross-section view. The inset of (b), the region indicated by a square in (b), shows the vertical growth more clearly. (c) HRTEM image of the nanowire grown on Ge (111). SAED pattern in upper right of (c) confirms that the growth direction of the nanowires is [111] (after [34])

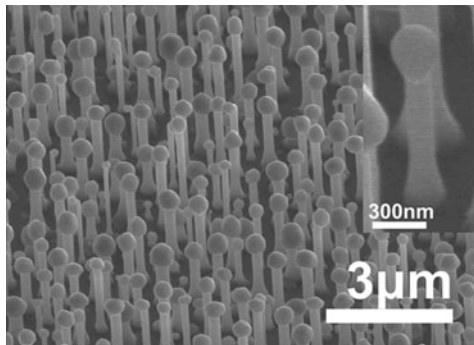
the availability of the same material as the substrate is a great advantage for a homoepitaxial relationship and vertical growth (refer Figs. 1.7 and 1.9).

Ge nanowires can also be grown vertically with a Ge substrate. For example, Kim et al. successfully grew Ge nanowires vertically on Ge(111) substrates by the VLS mechanism using Au as a catalyst [34]. As shown in Fig. 1.12a, most of the Ge nanowires grown on Ge[111] are arrayed vertically. Figure 1.12b and its inset also show SEM images of vertically grown Ge nanowires in a cross-section view, indicating the epitaxial growth of the nanowires in the [111] direction. In a structural analysis using HRTEM and SAED, the SAED pattern confirmed that the single-crystalline nanowires grew in the [111] direction (Fig. 1.12c).

As shown from the growth of Si and Ge nanowires, a homoepitaxial relationship is a rational approach for the vertical growth of nanowires. Therefore, the best way to achieve vertical growth of III–V or oxide nanowires is through the respective use of an III–V or oxide substrate. Figure 1.13 shows GaN nanowires grown vertically on GaN substrates (more precisely, GaN film deposited onto sapphire substrates). This figure indicates that the epitaxial relationship can be a success for the vertical growth of III–V nanowires by the VLS mechanism.

It should be noted that such substrates are not available in many cases. Furthermore, these types of substrates (e.g., GaN or ZnO) will raise the fabrication cost and thus complicate the mass production of devices. In this regard, the vertical growth

Fig. 1.13 Vertical growth of GaN nanowires on GaN film deposited sapphire substrate by establishing homoepitaxial relationship between nanowires and substrate. The growth direction of nanowires is same as the orientation of substrate, $\langle 0001 \rangle$



of nanowires through a heteroepitaxial relationship between the nanowires and substrates has been studied. For example, Kuykendall et al. grew a crystallographic alignment in high-density GaN nanowire arrays using LiAlO_2 or MgO [35]. It was revealed that the selection of single-crystal substrates is critical for achieving deterministic control of the growth direction; i.e., a close match of both the symmetry and lattice constant between the substrate and GaN is essential for successful heteroepitaxy, and this is anticipated to influence the nanowire growth direction strongly. For example, the oxygen sublattice in the (100) plane of γ - LiAlO_2 has twofold symmetry, which matches the twofold symmetry of the (100) plane of wurtzite GaN well. The lattice constants $a = 5.17 \text{ \AA}$ and $c = 6.28 \text{ \AA}$ of γ - LiAlO_2 represent a close match of the lattice constants $c = 5.19 \text{ \AA}$ and two times $a = 3.19 \text{ \AA}$ of GaN, respectively. In contrast, the (111) plane of MgO has threefold symmetry and an interatomic separation distance of 98 \AA for atoms in the (111) plane. This is a good match for the threefold symmetry of the (001) plane of GaN and the lattice constant $a = 3.19 \text{ \AA}$. As a result, these two substrates result in the selective growth of GaN nanowires in the $[1\bar{1}0]$ and $[001]$ directions, respectively. The growth of GaN nanowires vertically on sapphire or Si substrates has also been investigated [36,37].

Another area of study has been the vertical growth of other III–V group nanowires, such as GaAs and GaP. The approach for these nanowires is also based on the heteroepitaxial relationship. For example, GaP nanowires were grown vertically on Si substrates by utilizing a small lattice mismatch of less than 0.4% relative to Si [38]. It should be noted that epitaxial vertical growth was also achieved in the growth of GaAs nanowires on Si substrates with an interface with a larger lattice mismatch ($\sim 4.1\%$) [39]. A detailed analysis indicated that stacking faults in the nanowires influence the epitaxial growth of nanowires with a large mismatch. This implies that epitaxial growth can be achieved even under the condition of a large lattice mismatch between the nanowires and the substrate when a stress mediation mechanism is utilized.

Vertical growth of ZnO nanowires was achieved by utilizing a heteroepitaxial relationship. For example, ZnO nanowires can be grown vertically on the (110) plane of a sapphire substrate through matching with the (0001) plane of ZnO [40].

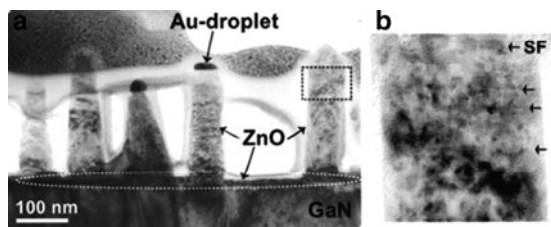


Fig. 1.14 (a) TEM cross-sectional image of the ZnO nanowires on the GaN substrate. A nearly continuous interfacial layer of ZnO separating vertical ZnO nanorods and GaN substrate is indicated using white dashed line. (b) Magnified view of the rectangular area in (a) (after [42])

Though the (110) plane of sapphire is symmetric by twofold and the ZnO c -plane is symmetric by sixfold, the a -axis of ZnO and the c axis of sapphire are mismatched at less than 0.08%. Such a coincidental matchup along the sapphire [0001] direction leads to the vertical heteroepitaxial growth of ZnO nanowires. Vertically aligned ZnO nanowires can also be grown on other substrates, for example, GaN, $\text{Al}_{0.5}\text{Ga}_{0.5}\text{N}$, and AlN substrates [41]. In these substrates, near-perfect vertical alignment of ZnO nanowires was observed, as both ZnO and the substrates have the same wurtzite structure and because the deposited ZnO nanowires are confined in their six equivalent $\langle 01\bar{1}0 \rangle$ directions and grow along the [0001] direction, following the substrate crystal orientation precisely.

Although a few studies have successfully demonstrated the vertical growth of III–V semiconductor and ZnO nanowires, it is also true that the vertical growth of nanowires was found to be unsuccessful in many studies. In those cases, it is unclear whether an epitaxial relationship between the nanowires and substrates was established because an interfacial layer typically formed between the nanowires and the substrate. These interfacial layers appear to have been deposited by the VS mechanism in advance of the growth of the nanowires by the VLS mechanism. Indeed, closer investigation of the interfaces between the ZnO nanowires and the GaN substrate showed this type of interface [42] (Fig. 1.14). This issue, the formation and effect of the interfaces, should be addressed in detail to achieve the heteroepitaxial as well as homoepitaxial vertical growth of nanowires.

One of the means of overcoming this difficulty is the activation of a metal catalyst for the VLS mechanism at a low temperature. Figure 1.15 shows the growth of GaN nanowires by the VLS mechanism. The left image shows nanowires grown using Ni as a catalyst. These grew randomly due to the formation of an interfacial layer. However, the right image shows the vertical growth of nanowires when using a cocatalyst, e.g., Au–Ni. This cocatalyst creates a liquid alloy at a low temperature and works as a VLS catalyst in advance of the deposition of the layer by the VS mechanism.

Coaxial heterostructure nanowire (COHN): The optical properties can be manipulated by creating COHN. For example, COHN can confine the photons as well as the electrons and thus yield improved performance of semiconductor lasers and LEDs with a variety of applications that require coherent light sources with low

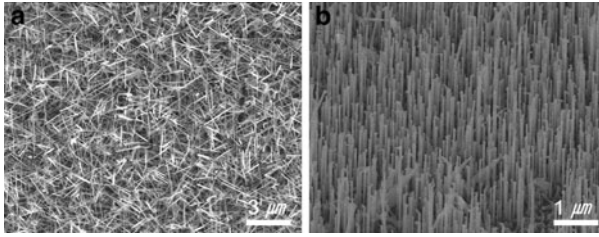


Fig. 1.15 Vertical growth of GaN nanowires on the GaN deposited sapphire substrate by VLS mechanism using cocatalyst on the substrate

power consumption and the capability of high-speed digital modulation. It is also ideal for photovoltaic cells due to the large junction area that extends along the entire length of the nanowire with carrier separation in the radial direction, which promises high efficiency. Furthermore, an electrical injection in COHN can be carried out efficiently with more flexibility in device designs that should be far superior to other structures for electrical injection optoelectronics [43].

Based on the VLS mechanism, COHN can be fabricated by two approaches. The first of these involves a combination of the VLS and VS mechanism in which nanowires using the VLS mechanism are initially grown in the longitudinal direction, after which a shell is deposited in the radial direction by the VS mechanism. A typical example of this approach is GaN/InGaN COHN multiquantum-well structures fabricated by the subsequent deposition of an In/AlGaIn layer on the surface of GaN nanowires grown by the VLS mechanism (Fig. 1.16) [44]. During this process, the composition of the shell is controlled by the temperature; a multiquantum-well structure with as many as 26 wells can be fabricated with COHN.

The other approach to fabricate COHN is through the use of a self-organization mode in a one-step VLS mechanism. Figure 1.17 shows GaN/AlGaIn COHN grown by spontaneous phase separation within the Ga–Al–N alloy nanowire system [45]. Bright-field transmission electron microscopy (BFTEM) images of the nanowire show a “dark” GaN core and a “bright” AlGaIn sheath along the axis of nanowires with smooth surfaces and sharp interfaces. The cores have diameters in the range of 5–40 nm, whereas the sheath thickness is in the range of 50–200 nm. The driving forces for this self-organizing process are the strain that develops in the nanowires. The curved surfaces of the materials are subjected to local pressure ΔP (and, in turn, stresses) according to the Laplace equation $\Delta P = \gamma[(1/r_1) + (1/r_2)]$, where r_1 and r_2 are two principal radii of curvature in a given point of a surface and γ is the surface tension. For nanowires, r_1 and r_2 correspond to the curvature in the radial and longitudinal directions, respectively; the former equals the radius of the nanowires, whereas the latter can be assumed to be infinite. Therefore, ΔP generated on the curved surface of the nanowires can be estimated as $\Delta P = \gamma/r_{\text{nanowire}}$, where r_{nanowire} is the nanowire radius. Owing to the positive curvature of the surfaces, compressive stresses in the inward radial direction arise and become significant

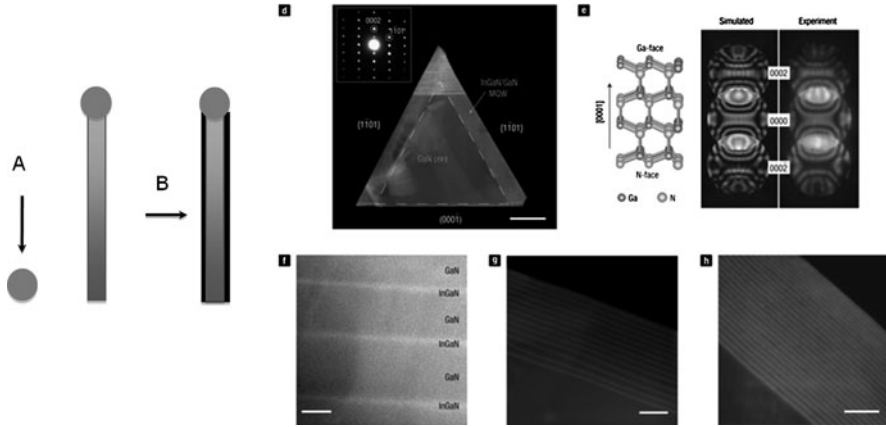


Fig. 1.16 (Left) Strategy for the fabrication of coaxial heterostructure nanowires by longitudinal growth by VLS mechanism followed by shell deposition by VS mechanism. A and B components are supplied for longitudinal growth and shell deposition, respectively (Right) Structural analysis of In/AlGaIn coaxial heterostructure nanowires (after [44])

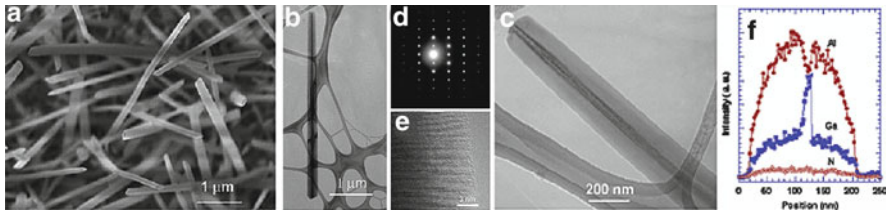


Fig. 1.17 GaN/AlGaIn COHN by self-organization mode. (a) SEM image of nanowires, (b)–(e) TEM images with diffraction pattern, (f) compositional analysis of nanowires (after [45])

as the size decreases. Similar phenomena can be found in the overgrowth of semiconductor alloy thin films, where spontaneous phase separation is accompanied by surface roughening (i.e., the formation of curved surfaces). Such a strain-induced self-ordering process can also lead to irregular spatial compositional modulation in the GaInAs nanowire system [46].

Si COHN can also be prepared in the self-organization mode. Figure 1.18 shows a TEM image of Si–Er COHN and a schematic illustration of the self-organization process for creating single-crystalline Si COHN arrays on (111) Si substrates [47]. In this mode, Si and Er are supplied to Au catalysts and form an Au–Si–Er alloy. One-dimensional epitaxial growth of nanowires then occurs with the precipitation of supersaturated Si and Er. Meanwhile, Er is extracted to the outside, where it reacts with oxygen and forms a Si–Er–O amorphous layer. An $\text{Er}_2\text{Si}_2\text{O}_7$ layer is then generated on the sheath by phase separation, leaving the amorphous SiO_2 layer inside. Further optical characterization showed strong luminescence with a wavelength of $1.54\ \mu\text{m}$. These outcomes indicate that COHN can be used to

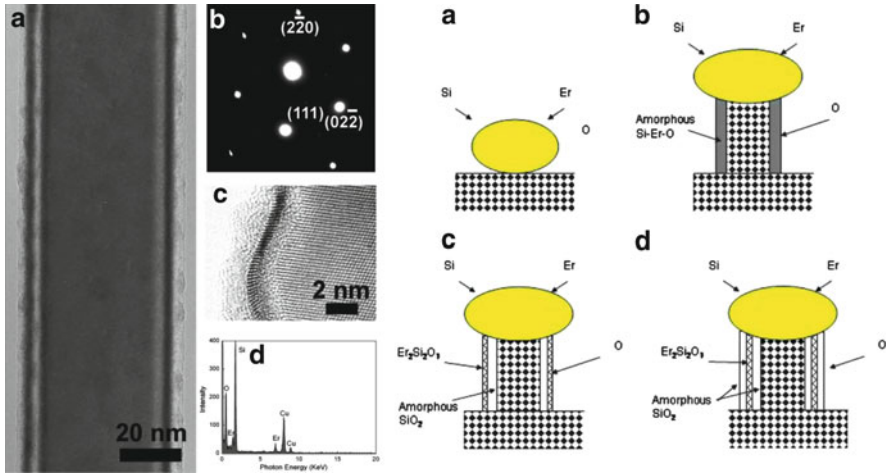


Fig. 1.18 (Left) TEM images of optically active COHN. (Right) The self-organization mechanism of COHN (after [47])

realize novel functionalities of semiconductor nanowires, for example, the optical activation of indirect-band-gap Si nanowires.

Longitudinal heterostructure nanowires (LOHN): The optical properties of nanowires can also be modulated through the fabrication of LOHN. For example, LOHNs can serve as quantum structures in the longitudinal direction that show enhanced optical properties due to the quantum confinement effect. The photoluminescence and electroluminescence can also be improved by creating a LOHN p-n junction [48].

LOHN can be prepared by the VLS mechanism with a catalyst or by using the VS mechanism without a catalyst, though only the former method is reviewed here. Figure 1.19 shows the strategy for the growth of LOHN involving the feeding of the components for the nanowires through a catalyst sequentially [48]. Figure 1.19 also shows TEM and EDS images of GaP/GaAs LOHN grown using this strategy. A compositional analysis showed that heterostructures were formed in the course of VLS growth. LOHNs of Si/SiGe and InAs/InP system could also be fabricated by this approach [49,50].

One of the issues related to the growth of LOHN by the VLS mechanism involves the interfaces between the heterostructures. Generally, optoelectronic devices require sharp interfaces in terms of their compositions or structures. However, the interfaces in LOHN using the VLS mechanism are typically not sharp enough due to the precipitation of the solid phase from the liquid phase, where the diffusion rate of the components is rather slow as compared to the vapor phase. Recent study, however, shows some promising results to overcome this limitation. Figure 1.20 (left) shows InAs/InP nanowire heterostructures that were grown with chemical beam epitaxy (CBE) on InAs (111) substrates using Au nanoparticles as a catalyst [51]. This figure shows very thin heterostructures in the longitudinal

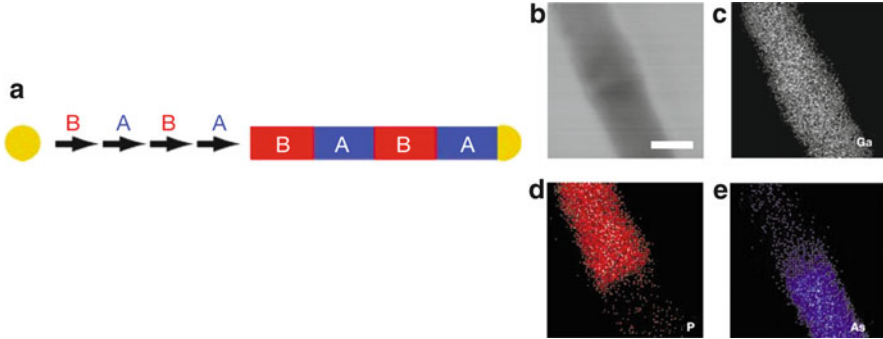
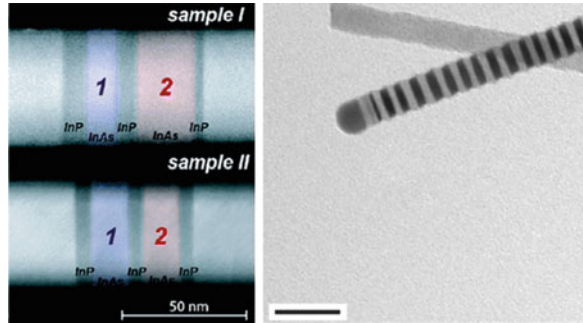


Fig. 1.19 (Left) Basic approach for the growth of longitudinal heterostructure nanowires using VLS mechanism. (Right) Compositional analysis of GaP/GaAs longitudinal heterostructure nanowires (after [48])

Fig. 1.20 (Left) TEM image of InAs/InP longitudinal heterostructure nanowires. (Right) TEM image of InP longitudinal heterostructure nanowires (after [51, 52])



direction that display a quantum confinement effect. Additionally, sharp interfaces were achieved by low growth rates together with the rapid switching of an indium source (TMIn). These abrupt changes between sections with different compositions, e.g., InAs, InP, or InAsP, along the nanowire with atomically sharp interfaces between them are typically challenging to achieve through the liquid phase. It is thus suggested that LOHN with sharp interfaces can be fabricated under controlled conditions.

Additionally, different approaches for the growth of LOHN have been studied [52]. Figure 1.20 (right) shows the InP superlattice of LOHN. To create heterostructures, InP nanowires were grown first from colloidal gold particles by the VLS mechanism. In the course of doing this, the nanowires grow in a zinc-blended crystal structure with a supply of diethyl zinc in a vapor form. When sufficient Zn is supplied, twin planes that exhibit constant spacing for a given Zn concentration and wire diameter appear, with twinning superlattice structures as a result. These LOHNs form because the doped Zn decreases the activation barrier for two-dimensional nucleation growth of zinc-blended InP and therefore promotes

the crystallization of the InP nanowires in the zinc-blend instead of the commonly found wurtzite crystal structure. It is not clear whether this approach can be applied to other semiconductor nanowires; however, it deserves further study as a new fabrication means of LOHN with sharp interfaces.

1.3.2.3 Compositional Modulation

Compositional modulation including alloying and doping is essential for the manipulation of the optical properties of semiconductor nanowires. For example, the photoluminescence or electroluminescence from III–V semiconductors can be tuned by modulating the composition in In–Al–Ga–N or In–Al–Ga–As in a quaternary-based system. The absorption of SiGe nanowires can be tuned by the composition in a binary-based system. This type of compositional modulation is thus important to exploit the potential of these materials in the area of optoelectronics.

Alloying of nanowires: IV and III–V semiconductors create a complete solid solution; thus, a binary, ternary, or quarterly alloy (e.g., $\text{Si}_{1-x}\text{Ge}_x$, $\text{In}_x\text{Ga}_{1-x}\text{As}$, or $\text{Al}_{1-x}\text{In}_y\text{Ga}_{1-x-y}\text{N}$) can be prepared. In line with this, compositional modulation of IV and III–V semiconductor nanowires has been studied.

The alloying of Si nanowires with Ge is readily achieved in the course of growth by the VLS mechanism. For example, $\text{Si}_{1-x}\text{Ge}_x$ alloy nanowires ($x = 0 \sim 0.3$) can be grown on Si (111) substrates using Au as a catalyst and SiCl_4 and Ge powders as precursors (Fig. 1.21) [53]. The resulting $\text{Si}_{1-x}\text{Ge}_x$ nanowires are well aligned on the substrates, and the diameter of these nanowires typically ranges from 50 to 100 nm. The composition of the $\text{Si}_{1-x}\text{Ge}_x$ nanowires can be varied by changing the growth temperature or the substrate distance (or both) from the Ge powder, which acts as a Ge precursor. Figure 1.21d shows a typical HRTEM image of the nanowires. The single-crystalline nature with a thin layer of native oxide can be seen in the HRTEM image. The SAED pattern recorded along the [001] zone axis, as shown in Fig. 1.21e, indicates that the nanowires grew in the [110] direction. Figure 1.21f shows the relative composition of Si and Ge in the $\text{Si}_{1-x}\text{Ge}_x$ nanowires through an EDS analysis, as shown for the $\text{Si}_{0.95}\text{Ge}_{0.05}$ and $\text{Si}_{0.7}\text{Ge}_{0.3}$ nanowires. This shows the compositional homogeneity of each nanowire with an EDS line scan. The profiles in both the radial and axial directions of the wire show that the composition of the native oxide is primarily SiO_x . No evidence of phase inhomogeneity was found (Fig. 1.21g, h); that is, no obvious Ge segregation within the nanowire was observed, as often found in thin film CVD. These outcomes imply that the alloying of Si and Ge was appropriate, leading to random substitutional alloy nanowires.

Alloying in III–V semiconductor nanowires is especially important in optoelectronic applications because it creates emissions with various wavelengths, from ultraviolet to the infrared region. Indeed, complete composition tunability of nanowires in the In–Ga–N system has been achieved [54]. In this study, single-crystalline $\text{In}_x\text{Ga}_{1-x}\text{N}$ nanowires across the entire compositional range from $x = 0$ to 1 were grown by low-temperature halide CVD. It also showed tunable emission

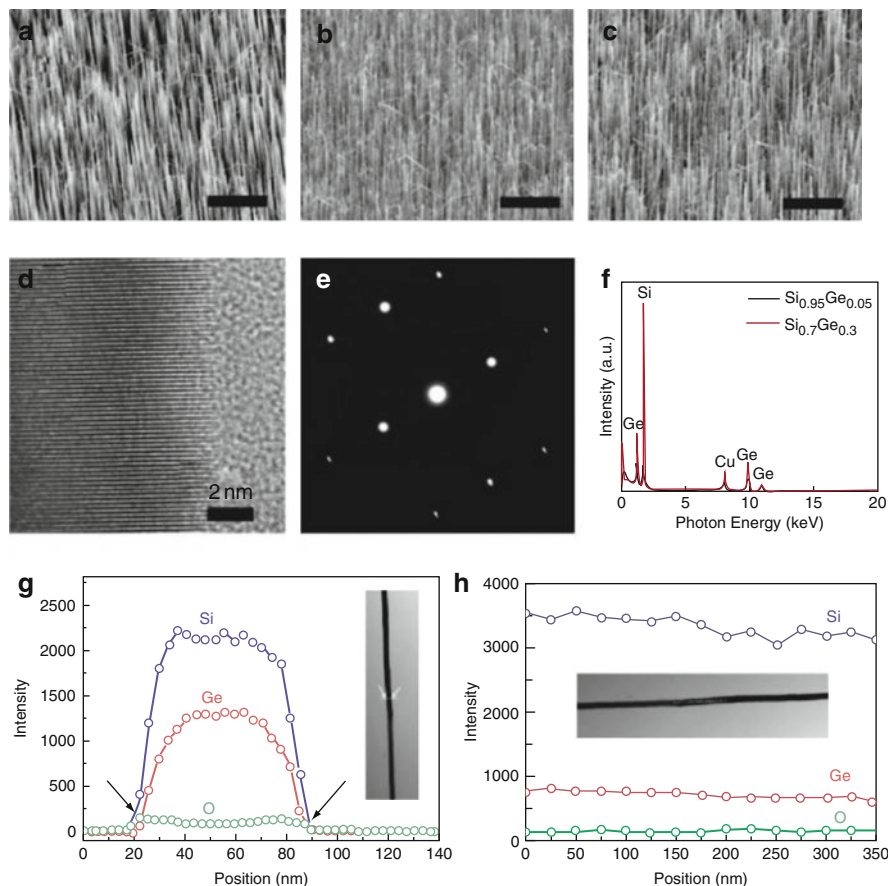


Fig. 1.21 $\text{Si}_{1-x}\text{Ge}_x$ nanowires grown by VLS mechanism. SEM images of (a) $\text{Si}_{0.95}\text{Ge}_{0.05}$, (b) $\text{Si}_{0.85}\text{Ge}_{0.15}$, (c) $\text{Si}_{0.7}\text{Ge}_{0.3}$ nanowires aligned on the Si (111) substrates, (d) Typical HRTEM image of controlled growth $\text{Si}_{1-x}\text{Ge}_x$ nanowires, showing the single-crystalline and defect-free nature, (e) SAED pattern, taken along the [001] zone axis that confirms the diamond structure of the wire with [110] growth direction, (f) typical EDS spectra of $\text{Si}_{0.95}\text{Ge}_{0.05}$ and $\text{Si}_{0.7}\text{Ge}_{0.3}$ nanowires. EDS line profiles in both radial (g) and axial (h) directions, showing that composition of native oxide is primarily SiO_x and any evidence of phase inhomogeneity is not found (after [53])

from the near-ultraviolet to the near-infrared region. However, these nanowires were grown without a catalyst. It should be noted that other studies pertaining to the alloying of III-N nanowires using the VLS mechanism have not been reported. This may be due to the difficulty of alloying of ternary- and quaternary-based systems through a liquid-metal phase. Unlike alloying directly from the vapor phase, the kinetics of alloying through the liquid phase is typically limited by the thermodynamics and kinetics of the system. However, our recent study demonstrates that compositional modulation of InGaAs nanowires can be achieved

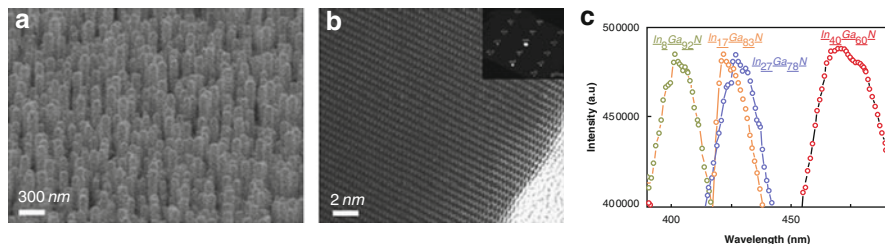


Fig. 1.22 InGaN nanowires grown by VLS mechanism and their PL. **(a)** SEM image of nanowires, **(b)** TEM image with diffraction pattern, **(c)** PL of InGaN nanowires with their composition

with the VLS mechanism. Figure 1.22 shows InGaN nanowires grown on a substrate using a cocatalyst of Au–Ni. The nanowires in this case grew on the substrate vertically. Figure 1.22b shows a typical HRTEM image of the nanowires. The single-crystalline nature can be seen in the HRTEM image. The SAED pattern recorded along the [001] zone axis, as shown in Fig. 1.22b, indicates that the nanowires grew in the [0001] direction. The PL measurements shown in Fig. 1.22c indicate that composition tunability and thus band-gap modulation is feasible through the VLS mechanism.

Alloyed InGaAs nanowires have been demonstrated by the VLS mechanism (Fig. 1.23). Kim et al. grew InGaAs nanowires using the VLS mechanism with Au as a catalyst [55]. Though the composition of these nanowires is not uniform along the longitudinal direction, their finding clearly indicates that compositional modulation can be achieved during the growth process.

Doping of nanowires: To realize electrical injection into a nanowire for optoelectronics, doping of electronic impurities is essential. The functionalization of nanowires for advanced optics, e.g., realizing magnetism in semiconductor nanowires for spin LEDs, also requires functional (e.g., magnetic) impurity doping.

Doping was previously demonstrated in Si nanowires [56]. The process is simple after supplying a dopant through vapor with a metal organic CVD precursor or the laser ablation of a solid target during the course of VLS growth. It results in n- and p-type Si nanowires. In a similar approach, Mg-doped, p-GaN nanowires can be prepared using magnesium nitride (Mg_3N_2) as a Mg source [37]. In this study, the doping concentration was controlled by changing the separation distance between the doping source and the substrate (Fig. 1.24, left). As shown in Fig. 1.24 (right), this was effective and changed the resistance of the nanowires.

In addition to electronic impurities, the doping of functional impurities has been studied. One typical example is magnetic impurity doping into semiconductor nanowires to realize magnetism in the semiconductor and spin-related optoelectronics. Regarding this, Mn was doped into Ge nanowires by transporting germanium chloride (GeCl_4) and manganese dichloride (MnCl_2) onto an Au-coated silicon substrate [34]. Despite the Mn doping, an analysis revealed that the nanowires maintain their single-crystalline nature without defects or secondary phases. Compositional

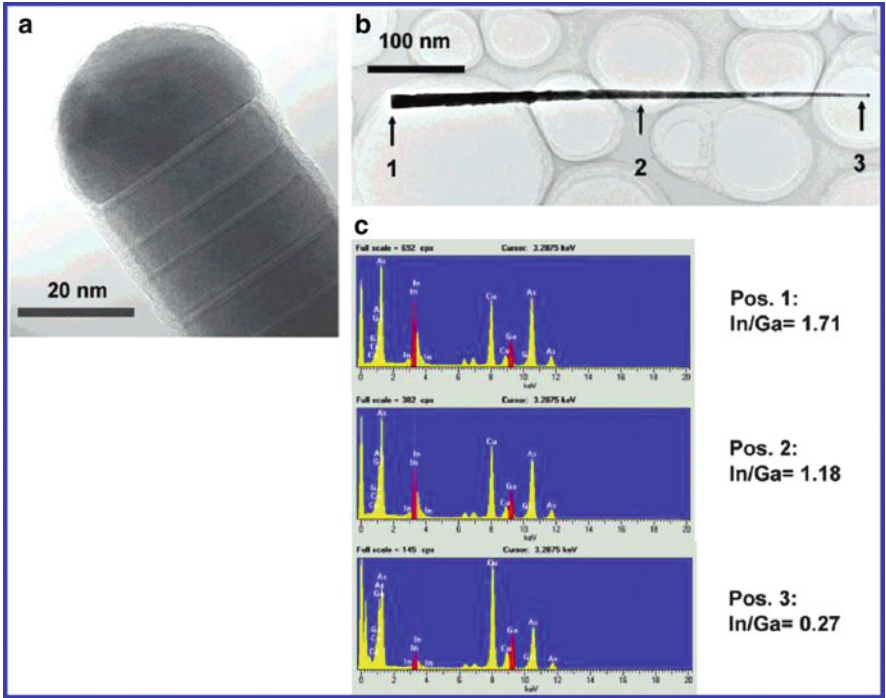


Fig. 1.23 InGaAs nanowires grown by VLS mechanism (after [55])

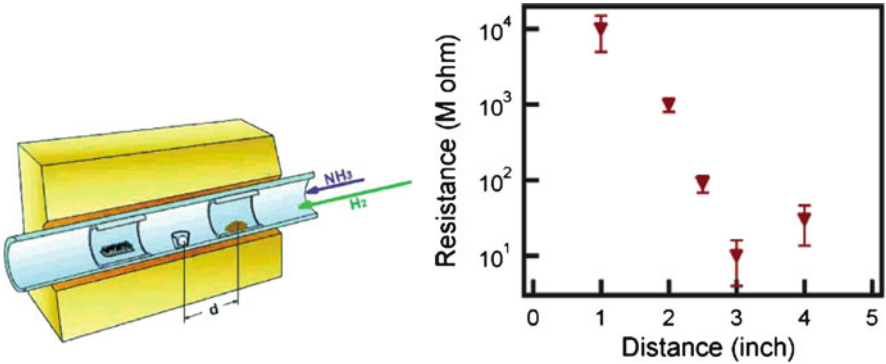


Fig. 1.24 (Left) Schematic for the apparatus for doping of GaN nanowires. (Right) The resistance of nanowires as a function of separation between doping source and substrate (after [37])

analysis indicated that the average Mn concentration measured from ten nanowires was ca. 1.5%. This result indicates that magnetic impurities can be doped into IV semiconductor nanowires by the VLS mechanism. Magnetic impurity doping into GaN nanowires was also achieved. For example, Seong et al. doped Mn or Cu in GaN nanowires up to several at% without sacrificing the single-crystalline nature by using the VLS mechanism [57, 58]. In these works, single-crystalline magnetic semiconductor $\text{Ga}_{1-x}\text{Cu(or Mn)}_x\text{N}$ nanowires were synthesized using a Ni catalyst deposited onto c-plane sapphire substrates in a chemical vapor transport system. Solid metallic Ga and Cu(or Mn)Cl powder, and NH_3 were used as the Ga and dopant and nitrogen source. Figure 1.25a shows an SEM image of GaCuN nanowires grown on the substrate. The diameter and length of these nanowires are from 10 to 100 nm and tens of micrometers, respectively, and they have a triangular structure (inset in Fig. 1.25a). Figure 1.25d shows an HRTEM image. The single-crystalline nature without defects or secondary phases can be seen in all of the HRTEM images. The SAED pattern of the wire, as shown in Fig. 1.25b, indicates that the nanowires grew in the $[1-100]$ direction, perpendicular to the (1000) crystal plane. Figure 1.25c shows the representative Cu concentration as determined by an EDS analysis. The average Cu concentration measured from ten nanowires was ca. 1 to 4% depending on the processing conditions. Further characterization indicates that room-temperature ferromagnetism was achieved from Cu- or Mn-doped GaN semiconductor nanowires. These outcomes demonstrate that n- and p-doping as well as magnetic doping with large ions can be achieved. It should be noted that a high level of doping as compared to thin films can be achieved in the nanowires. This may be due to uniaxial stress in the nanowires, which may be attributed to higher solubility to dopants.

Although limited studies successfully showed the doping of nanowires, doping nonetheless remains a challenging issue owing to the lack of any background on the incorporation of impurities into nanowires. In this regard, Perea et al. carried out atomic-scale direct measurements of dopant concentrations in arbitrary regions of individual nanowires using atomic probe tomography [59]. They found that differences in precursor decomposition rates between the liquid catalyst and the solid nanowire surface give rise to a heavily doped shell surrounding an under doped core (Fig. 1.26). This finding shows that doping in nanowires is different from bulk and thin films and thus requires additional characterization to accumulate the quantitative data necessary to understand the doping mechanism in many different types of nanowires.

1.4 Devices Based on the VLS Mechanism

Based on the VLS mechanism, nanowire optoelectronics can be developed, given that many conceptual devices have already been demonstrated. These conceptual devices were investigated based on a single nanowire or an array of nanowires. Single-nanowire devices are fabricated by the process as follows. First, the

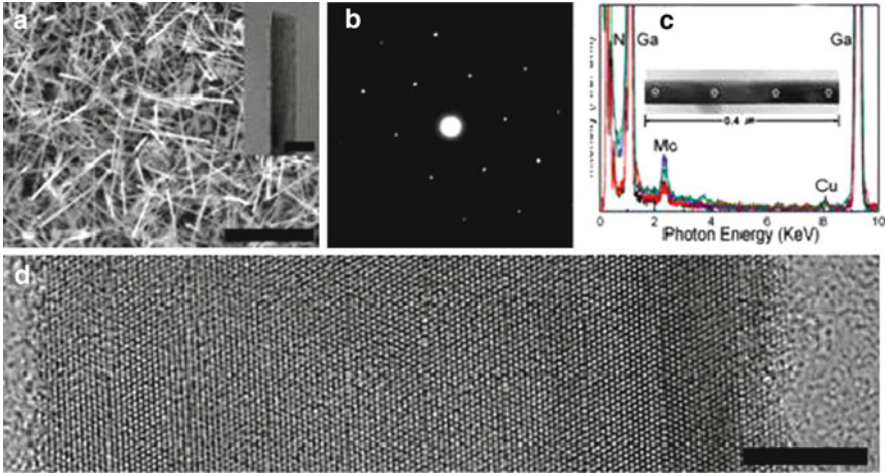
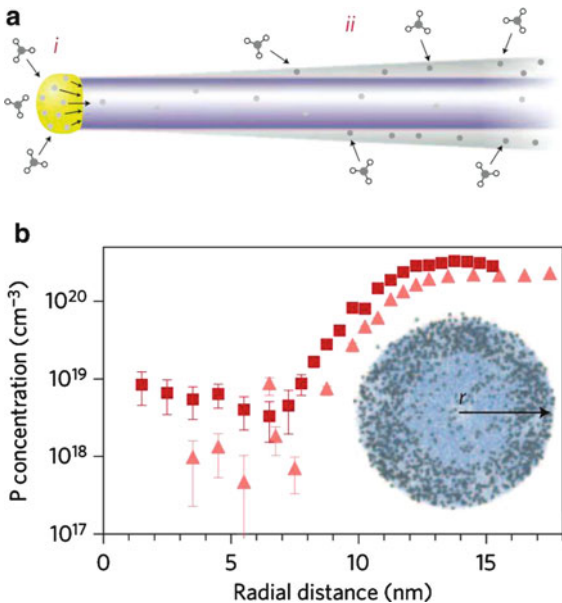


Fig. 1.25 Synthesis and structural characterization of $\text{Ga}_{1-x}\text{Cu}_x\text{N}$ nanowires. (a) Typical SEM image of $\text{Ga}_{1-x}\text{Cu}_x\text{N}$ nanowires grown on the sapphire substrate. *Inset* is TEM image of the nanowire showing a triangular structure. The *scale bars* in (a) and *inset* are $5\mu\text{m}$ and 50 nm , respectively. (b) SAED pattern of the nanowire, recorded on the $[0001]$ zone axis. (c) EDS spectra collected from different positions within the $\text{Ga}_{1-x}\text{Cu}_x\text{N}$ nanowires as marked with O. *Inset* is a TEM image of a nanowire. The spectra show essentially the same compositions without any evidence of phase inhomogeneity. (d) HRTEM image of a nanowire with diameter of 50 nm . The *scale bar* is 2 nm (after [58])

Fig. 1.26 Dopant incorporation pathways and distribution. (a) Schematic representation of dopant incorporation pathways via the catalyst (i) and surface decomposition (ii). (b) Radial plot of phosphorus concentration for germanium nanowires. The *inset* shows the path along which the concentration was measured (after [59])



nanowires are grown on the substrate. The nanowires are then dispersed in a liquid medium and assembled *ex situ* on the substrates, where the electrodes are prepatterned. Fabrication of the top electrodes, serving as a passivation layer, is then carried out to the degree necessary. A typical illustration can be found in the preparation of InP nanowire optoelectronic devices [60]. In this process, InP nanowires were grown using Au as a catalyst, and Te and Zn were added as precursors at 1%. After the growth, the nanowires were collected and dispersed in ethanol and then deposited onto oxidized silicon substrates, with conductive silicon used as a back gate. Electrical contact for the NWs was done using electron beam lithography. Ni/In/Au contact electrodes were then thermally evaporated. By this process, a single-nanowire device can be fabricated. Moreover, to fabricate cross-nanowires as a junction structure, layer-by-layer deposition was used. In this process, first a dilute solution of one type of nanowire is deposited on the substrate and the positions of individual nanowires are recorded. In the second step, a dilute solution of another type (for example, p-type) of nanowires is deposited, and the positions of the crossed n- and p-type nanowires are recorded. Metal electrodes are then defined. The inset in Fig. 1.27b shows the crossed nanowire p-n junction, while Fig. 1.27 shows an optical image of the electroluminescence characteristics of the junction.

By further modulating the nanowires during the course of their growth, more versatile devices can be fabricated. One example is the multicolor emission of a nanowire LED [61]. Figure 1.28a shows the concept of single-nanowire structures that consist of an inner n-type GaN core and sequentially deposited i-InGaN, i-GaN, p-AlGaIn, and p-type GaN shells for modulation of the luminescence. In this structure, the n-type GaN core and the p-type GaN outer shell serve as electron and hole injection layers, respectively. The $\text{In}_x\text{Ga}_{1-x}\text{N}$ layer provides a tunable band gap as well for the efficient radiative recombination of injected carriers, while the wider band gap and lower index of refraction of the AlGaIn cladding layer can enhance the confinement of both carriers and photons in the InGaIn active layer. Based on this concept, n - GaN/ $\text{In}_x\text{Ga}_{1-x}\text{N}$ /GaN/p - AlGaIn/p - GaN nanowire radial heterostructures were grown by longitudinal growth using a catalyst followed by controlled shell deposition onto the nanowire core. During the deposition process, the composition of the InGaIn layer was systematically tuned and could therefore be used to define the band gap of the InGaIn and the corresponding emission energy. Through these modulations, the nanowire devices yielded electroluminescence (EL) with red shifts in their emission peak after increasing the In composition with high quantum efficiency. This approach was also used for the growth of a single COHN for photovoltaic cells [62].

Nanowire array optoelectronic devices were fabricated in an *in situ* mode using the as-grown nanowires on the substrates. Figure 1.29 shows the typical process of the fabrication of a nanowire array for optoelectronics, such as LEDs [57]. The process starts with the growth of the nanowires on the substrates. In this step, the nanowires can be modulated structurally (e.g., diameter control) or compositionally (e.g., doping of electronic or magnetic impurities) to improve the performance of the device. In the example in Fig. 1.29, quasivertically aligned GaN nanowires

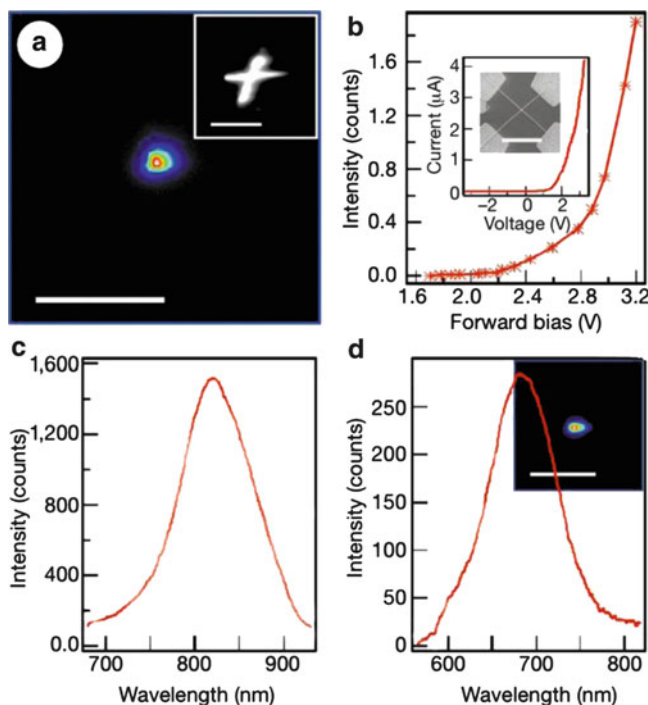


Fig. 1.27 Optoelectrical characterization of nanowire p-n junctions. (a) Electroluminescence (EL) image of the light emitted from a nanowire p-n junction. *Inset*: photoluminescence (PL) image of the junction, (b) EL intensity versus voltage. *Inset*: $I \pm V$ characteristics, (c) EL spectrum of the junction shown in (a), (d) EL spectrum recorded from a second forward-biased crossed nanowire p-n junction. *Inset*: EL image showing that the EL originates from the junction region (after [60])

were grown on n-SiC (0001) substrates using Ni catalysts (Fig. 1.29a). Here, an n-SiC substrate was used to construct a p-n junction between the nanowires and the substrates and also for the alignment of the GaN nanowires. During the growth process, the nanowires were compositionally modulated by doping with Mn to achieve magnetism as well as p-type characteristics. Therefore, the p-n junctions formed at the interface between the nanowires and the substrates while the diameter and length were controlled by the thickness of the Ni films and the growth time. The fabrication of electrodes on top of the nanowires and on the bottom of the substrates for electrical injections was done subsequent to the growth process. In this case, ohmic contacts were achieved by evaporating Ni/Au and Ni bilayers on the nanowires and substrates, respectively, followed by rapid thermal annealing. Transport measurements showed well-defined current rectification characteristic of p-n diodes (Fig. 1.29c). The I - V data recorded from the nanowires and substrate were symmetric and thus can attribute the rectification to the p-n junction between the nanowires and substrate and not to the junction between the nanowires and

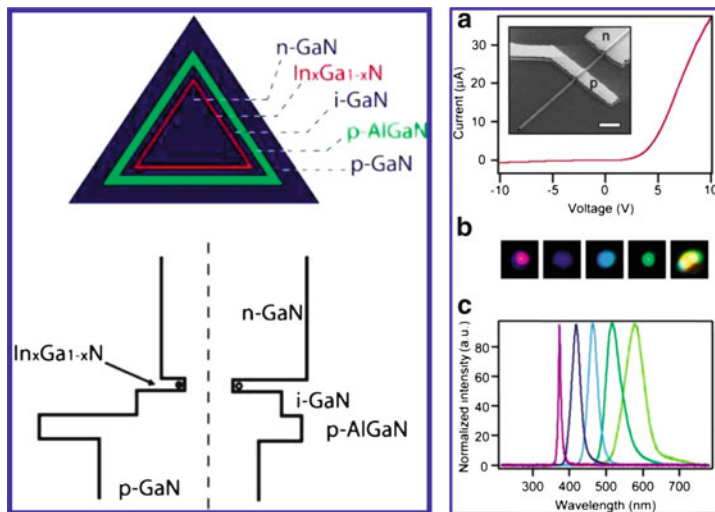


Fig. 1.28 (Left) Cross-sectional view of a nanowire heterostructure and the corresponding energy band diagram. (Right) (a) Current versus voltage data recorded on a nanowire device. *Inset*: field emission scanning electron microscopy image of a representative nanowire device. (b) Optical microscopy images collected from around p-contact of nanowire LEDs in forward bias, showing purple, blue, greenish-blue, green, and yellow emission, respectively. (c) Normalized EL spectra recorded from five representative forward-biased multicolor nanowire LEDs (after [61])

the metal contacts. Electroluminescence spectra measurements of these junctions showed a dominant emission peak centered at 430 nm, which is consistent with the PL of the nanowires (Fig. 1.29e).

A good example that shows a combination of the CMOS process with the structural and compositional modulation of nanowires for realizing nanowire-based LEDs is contained in the report by Severson et al. [63] (Fig. 1.30). In this work, i-GaAs nanowires were grown on a p-Si/p-GaP substrate vertically by the VLS mechanism using Au as catalyst. The GaAs nanowires were grown vertically on the GaP and Si substrates due to the epitaxial relationship between the nanowires and the substrates (Fig. 1.31). For the positioning of the nanowires, standard lithography techniques were used. After the growth of the nanowires, InGaP shells with n-type doping were deposited on the surface of the nanowires and p-i-n junction structures were then formed in the nanowires. The fabrication of the electrodes was done via a standard CMOS process. The established LED functionality of these devices demonstrated that modulation of nanowires by the VLS mechanism can be carried out in the CMOS process for advanced optoelectronics.

Other optoelectronic devices can be developed based on the VLS mechanism. For example, the growth of III-V nanowires on Si has also been demonstrated for the fabrication of GaN nanowire-based solar cells. In this study, vertically aligned Mg-doped GaN nanorods were epitaxially grown on an n-type Si substrate. The result showed a good high-photocurrent density, high-energy conversion efficiency,

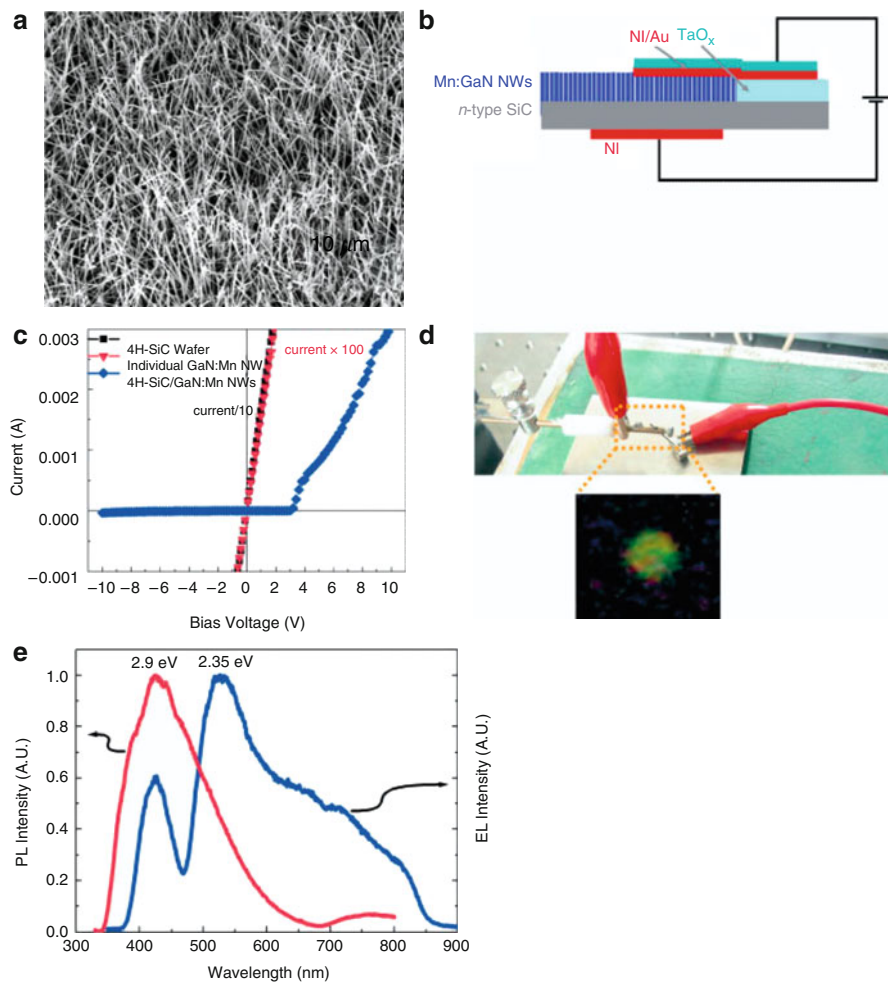


Fig. 1.29 GaN:Mn nanowire LED. (a) SEM image of the quasivertical nanowire arrays on substrate, (b) schematic illustration of the LED structures, (c) I - V behavior of n-SiC substrate/GaN:Mn nanowire junction, (d) image of light-emitting interface. *Top* and *bottom* images show the device configuration of the nanowire-based LED structure and an optical image of the emitting device, respectively, (e) EL spectrum from nanowire LED, and PL spectrum from GaN:Mn nanowires measured at room temperature using He-Cd laser as excitation source (after [57])

and reduced light loss due to reflection [64]. Though the interfaces were not clearly characterized, this outcome also demonstrates that vertically aligned nanowire p-n junctions can be fabricated by the VLS mechanism. A Si nanowire-based photodetector has also been investigated similarly through the growth of Si nanowires on a substrate, and a photodetector was fabricated in a manner similar to that used with LED or photovoltaic cells [65].

1.5 Summary and Perspectives

The VLS mechanism has been successfully used for the growth of nanowires for optoelectronics. The uniqueness that has made this mechanism a mainstay for the growth of nanowires is its simplicity. The VLS mechanism can be realized by simply adding a metal catalyst to the crystal growth process. Therefore, it can be easily adapted in many conventional semiconductor fabrication processes. Because this mechanism has been rediscovered for the growth of nanowires, most of the studies related to it have investigated metal catalysts to the point that this mechanism is now considered a general method that can be used for the growth of various nanowires. The feasibility of the structural and compositional modulation of nanowires further fuels this mechanism as workhorse in this field.

However, it is true that several issues have to be addressed before the potential of the VLS mechanism can be exploited in the future. One of these issues is the establishment of the nanothermodynamics and kinetics for the nanoliquid–solid system. The thermodynamic and kinetic data from bulk materials have been used to explain the growth of nanowires thus far. However, the growth that occurs in nanosystems in which the thermodynamics and kinetics are different is itself quite different to that in bulk systems. Therefore, frameworks such as size effect on the phase relationship, role of surface energy on the stability of 1D nanostructures, and diffusion kinetics in liquid on a nanometer scale have to be established. Such fundamentals are essential to grow nanowires rationally. It can also pave the way for the preparation of nanowires in an unprecedented size range of sub-10 nm. The compatibility of metal catalysts to the CMOS process should be addressed for device fabrication. Though nanowires can be grown easily with a metal catalyst in a semiconductor fabrication process, some of them are not compatible with the CMOS process. The possible unintended contamination of a catalyst component in nanowires should also be addressed. A few studies have been done on this issue; however, more quantitative data have to be published to overcome this issue

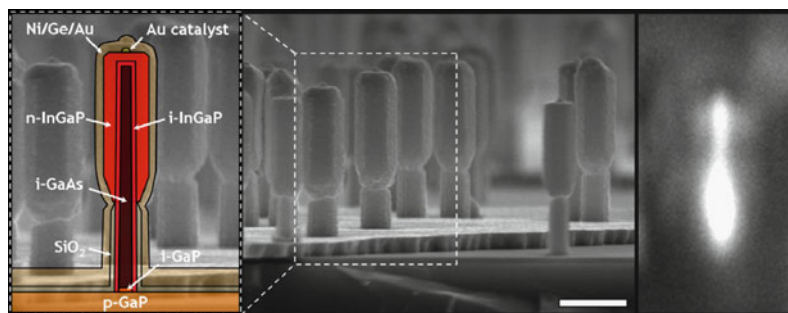


Fig. 1.30 Side-view scanning electron microscopy (SEM) image showing nanowire LEDs. *Left inset:* sketch drawing of the device structure. *Right inset:* side-view CCD camera image showing electroluminescence (EL) from a single-nanowire LED structure (after [63])

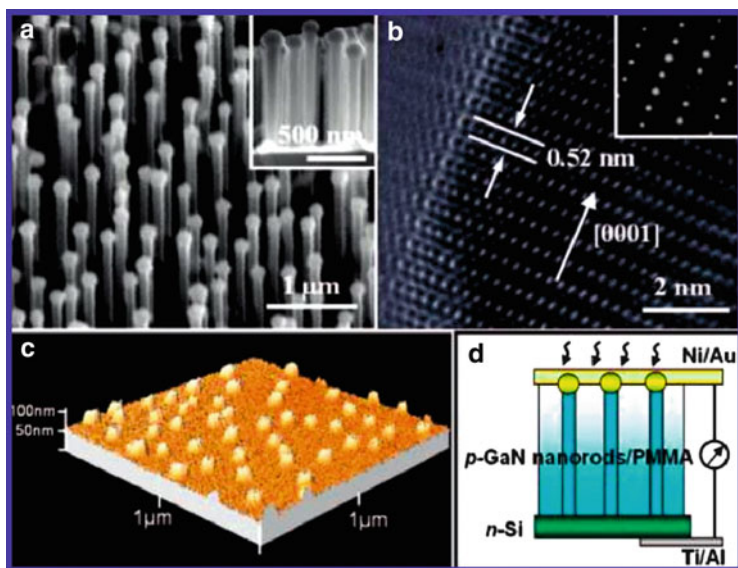


Fig. 1.31 (a) Tilt top view SEM image of Mg-doped GaN nanorod arrays. *Inset* shows cross-sectional SEM image. (b) HRTEM image of GaN nanorod and its corresponding SAED pattern (*inset*). (c) AFM image of GaN nanorod tips exposed above the photoresist layer. (d) A schematic of the p-GaN nanorod/n-Si heterojunction photovoltaic cell (after [64])

and in turn to achieve the better optical properties of nanowires. Regarding these, the correlation of the final optical properties with the structure and composition of nanowires may reveal the more sensitive processing parameters for the VLS mechanism. These parameters can be studied quantitatively as well as qualitatively to establish the growth process of nanowires in a predictable, reliable manner for optoelectronic applications. The scaling up of the growth process is another issue that should be addressed. This issue has not been investigated thoroughly as yet; however, this will be important for the industrialization of nanowires near future. To achieve this, the many steps required for the growth of nanowires should be standardized to achieve reliability of the growth process.

Since the 1990s, the VLS mechanism has played a critical role in the creation of the science of nanowires, which has fueled the advance in many optoelectronic fields. The many studies carried over the past two decades have built the foundation of the great potential of this mechanism. To step forward in this area, the mechanism has to be developed from the point of view of industrialization of the nanowires. It will fuel the scientific research in the field of nanowires as well as the creation of advanced optoelectronic market.

Acknowledgements This work was supported by a grant from the National Research Laboratory program and Pioneer Program through the Korea Science and Engineering Foundation funded by the Ministry of Education, Science & Technology.

References

1. S. Wagner, W.C. Ellis, Appl. Phys. Lett. **4**, 89 (1964); in *Whisker Technology*, ed. by A.P. Levitt (John Wiley and Sons, Inc., New York, 1970)
2. H.-J. Choi, J.-G. Lee, J. Mat. Sci. **30**, 1982 (1995)
3. Y. Wu, P. Yang, J. Am. Chem. Soc. **123**, 3165 (2001)
4. F.M. Ross, J. Tersoff, M.C. Reuter, Phys. Rev. Lett. **95**, 146104 (2005)
5. V. Schmidt, J.V. Wittemann, S. Senz, U. Gosele, Adv. Mat. **21**, 2681 (2009)
6. T.B. Massalski, P.R. Submanian, H. Okamoto, *Binary Alloy Phase Diagrams*, 2nd ed., vol. 1 (ASM International, Materials Park, OH, 1998)
7. E.A. Sutter, P.W. Sutter, ACS Nano **4**, 4943 (2010)
8. H. Adhikari, A.F. Marshall, I.A. Goldthorpe, C.E.D. Chidsey, P.C. McIntyre, ACS Nano **1**, 415 (2007)
9. E.J. Schwalbach, P.W. Voorhees, Nano Lett. **8**, 3739 (2008)
10. S. Kodambaka, J. Tersoff, M.C. Reuter, F.M. Ross, Science **316**, 729 (2007)
11. E.I. Givargozov, J. Cryst. Growth **31**, 20 (1975)
12. T.I. Kamins, R.S. Williams, D.P. Basile, T. Hesjedal, J.S. Harris, J. Appl. Phys. **89**, 1008 (2001)
13. K. Lew, J.M. Redwing, J. Cryst. Growth **254**, 14 (2003)
14. J. Kikkawa, Y. Ohno, S. Takeda, Appl. Phys. Lett. **86**, 123109–1 (2005)
15. M.H. Huang, Y. Wu, H. Feick, N. Tran, E. Weber, P. Yang, Adv. Mat. **13**, 113 (2001)
16. H. Jeong, T.E. Park, H.K. Seong, M. Kim, U. Kim, H.J. Choi, Chem. Phys. Lett. **467**, 331 (2009)
17. T. Stelzner, G. Andra, E. Wendler, W. Wesch, R. Scholz, U. Gosele, S. Christiansen, Nanotechnology **17**, 2895 (2006)
18. J.E. Allen, E.R. Hemesath, D.E. Perea, J.L. Lensch-Falk, Z. Y. Li, F. Yin, M.H. Gass, P. Wang, A.L. Bleloch, R.E. Palmer, L.J. Lauhon, Nat. Nanotechnol., **3**, 168. (2008)
19. J.B. Hannon, S. Kodambaka, F.M. Ross, R.M. Tromp, Nature **440**, 69 (2006)
20. Y. Ke, X. Weng, J.M. Redwing, C.M. Eichfeld, T.R. Swisher, S.E. Mohny, Y.M. Habib, Nano Lett. **9**, 4494 (2009)
21. Y. Wang, V. Schmidt, S. Senz, U. Gosele, Nat. Nanotechnol. **1**, 186 (2006)
22. P.X. Gao, Y. Ding, Z.L. Wang, Nano Lett. **3**, 1315 (2003)
23. J. Yoo, Y.-J. Hong, S. An, G.-C. Yi, B. Chon, T. Joo, J.-W. Kim, J.-S. Lee, Appl. Phys. Lett. **89**, 043124–1 (2006)
24. B. Mandl, J. Stangl, E. Hilner, A.A. Zakharov, K. Hillerich, A.W. Dey, L. Samuelson, G. Bauer, K. Deppert, A. Mikkelsen, Nano Lett. **10**, 4443 (2010)
25. L. Gao, R.L. Woo, B. Liang, M. Pozuelo, S. Prikhodko, M. Jackson, N. Goel, M.K. Hudait, D.L. Huffaker, M.S. Goorsky, S. Kodambaka, R.F. Hicks, Nano Lett. **9**, 2223 (2009)
26. B. Delley, E.F. Steigmeier, Appl. Phys. Lett. **67**, 2370 (1995)
27. C. Harris, E.P. O'Reilly, Physica E **32**, 341 (2006)
28. Y. Wu, Y. Cui, L. Huynh, C.J. Barrelet, D.C. Bell, C.M. Lieber, Nano Lett. **4**, 433 (2004)
29. J. Goldberger, R. He, Y. Zhang, S. Lee, H. Yan, H.-J. Choi, P. Yang, Nature **422**, 599 (2003)
30. M.S. Gudiksen, J. Wang, C.M. Lieber, J. Phys. Chem. B **106**, 4036 (2002)
31. X. Wang, Y. Ding, C.J. Summers, Z.L. Wang, J. Phys. Chem. B **108**, 8773 (2004)
32. L. Cao, J.S. White, J.-S. Park, J.A. Schuller, B.M. Clemens, M.L. Brongersma, Nat. Mater. **8**, 643 (2009)
33. L. Hu, G. Chen, Nano Lett. **7**, 3249 (2007)
34. U. Kim, T.-E. Park, I. Kim, H.-K. Seong, M.-H. Kim, J. Chang, J.-G. Park, H.-J. Choi, J. Appl. Phys. **106**, 123903–1 (2009)
35. T. Kuykendall, P.J. Pauzauskie, Y. Zhang, J. Goldberger, D. Sirbully, J. Denlinger, P. Yang, Nat. Mater. **3**, 524 (2004)
36. Y.B. Tang, Z.H. Chen, H.S. Song, C.S. Lee, H.T. Cong, H.M. Cheng, W.J. Zhang, I. Bello, S.T. Lee, Nano Lett. **8**, 4191 (2008)

37. Z. Zhong, F. Qian, D. Wang, C.M. Lieber, *Nano Lett.* **3**, 343 (2003)
38. T. Mårtensson, C.P.T. Svensson, B.A. Wacaser, M.W. Larsson, W. Seifert, K. Deppert, A. Gustafsson, L.R. Wallenberg, L. Samuelson, *Nano Lett.* **4**, 1987 (2004)
39. X.-Y. Bao, C. Soci, D. Susac, J. Bratvold, D.P.R. Aplin, W. Wei, C.-Y. Chen, S.A. Dayeh, K.L. Kavanagh, D. Wang, *Nano Lett.* **8**, 3755 (2008)
40. M.H. Huang, S. Mao, H. Feick, H. Yan, Y. Wu, H. Kind, E. Weber, R. Russo, P. Yang, *Science* **292**, 1897 (2001)
41. X. Wang, J. Song, P. Li, J.H. Ryou, R.D. Dupuis, C.J. Summers, Z.L. Wang, *J. Am. Chem. Soc.* **127**, 7920 (2005)
42. I. Levin, A. Davydov, B. Nikoobakht, N. Sanford, P. Mogilevsky, *Appl. Phys. Lett.* **87**, 103110-1 (2005)
43. D. Li, C.Z. Ning, *Nano Lett.* **8**, 4234 (2008)
44. F. Qian, Y. Li, S. Gradecak, H. Park, Y. Dong, Y. Ding, Z. Wang, C.M. Lieber, *Nat. Mater.* **7**, 791 (2008)
45. H.-J. Choi, J.C. Johnson, R. He, S.-K. Lee, F. Kim, P. Pauzauskie, J. Goldberger, R.J. Saykally, P. Yang, *J. Phys. Chem. B*, **107**, 8721 (2003)
46. P.D. Markowitz, M.P. Zach, P.C. Gibbons, R.M. Penner, W.E. Buhro, *J. Am. Chem. Soc.* **123**, 4502 (2001)
47. H.-J. Choi, J.H. Shin, K. Suh, H.-K. Seong, H.-C. Han, J.-C. Lee, *Nano Lett.* **5**, 2432 (2005)
48. M.S. Gudiksen, L.J. Lauhon, J. Wang, D.C. Smith, C.M. Lieber, *Nature* **415**, 617 (2002)
49. M.T. Bjork, B.J. Ohlsson, T. Sass, A.I. Persson, C. Thelander, M.H. Magnusson, K. Deppert, L.R. Wallenberg, L. Samuelson, *Nano Lett.* **2**, 87 (2002)
50. Y. Wu, R. Fan, Peidong Yang, *Nano Lett.*, **2**, 83 (2002)
51. A. Fuhrer, L.E. Froberg, J.N. Pedersen, M.W. Larsson, A. Wacker, M.-E. Pistol, L. Samuelson, *Nano Lett.* **7**, 243 (2007)
52. R.E. Algra, M.A. Verheijen, M.T. Borgstrom, L. Feiner, G. Immink, W.J.P. VanEnckevort, E. Vlie, E.P.A.M. Bakkers, *Nature*, **456**, 369-372 (2008)
53. H.-K. Seong, E.-K. Jeon, M.-H. Kim, H. Oh, J. Lee, J.-J. Kim, H.-J. Choi, *Nano Lett.* **8**, 3656 (2008)
54. T. Kuykendall, P. Uurich, S. Aloni, P. Yang, *Nat. Mater.* **6**, 951 (2007)
55. Y. Kim, H.J. Joyce, Q. Gao, H.H. Tan, C. Jagadish, M. Paladugu, J. Zou, A.A. Suvorova, *Nano Lett.* **6**, 599 (2006)
56. Y. Cui, X. Duan, J. Hu, C.M. Lieber, *J. Phys. Chem. B* **104**, 5213 (2000)
57. H.-J. Choi, H.-K. Seong, J. Chang, K.-I. Lee, Y.-J. Park, J.-J. Kim, S.-K. Lee, R. He, T. Kuykendall, Peidong Yang, *Adv. Mater.* **17**, 1351 (2005)
58. H.-K. Seong, J.-Y. Kim, J.-J. Kim, S.-C. Lee, S.-R. Kim, U. Kim, T.-E. Park, H.-J. Choi, *Nano Lett.* **7**, 3366 (2007)
59. D.E. Perea, E.R. Hemesath, E.J. Schwalbach, J.L. Lensch-Falk, P.W. Voorhees, L.J. Lauhon, *Nat. Nanotechnol.* **4**, 315 (2009)
60. X. Duan, Y. Huang, Y. Cui, J. Wang, C.M. Lieber, *Nature* **409**, 66 (2001)
61. F. Qian, S. Gradecak, Y. Li, C.-Y. Wen, C.M. Lieber, *Nano Lett.* **5**, 2287 (2005)
62. Y. Dong, B. Tian, T.J. Kempa, C.M. Lieber, *Nano Lett.* **9**, 2183 (2009)
63. C.P.T. Svensson, T. Martensson, J. Tragardh, C. Larsson, M. Rask, D. Hessman, L. Samuelson, *J. Ohlsson, Nanotechnology* **19**, 305201 (2008)
64. Y.B. Tang, Z.H. Chen, H.S. Song, C.S. Lee, H.T. Cong, H.M. Cheng, W.J. Zhang, I. Bello, S.T. Lee, *Nano Lett.* **8**, 4191 (2008)
65. J. Bae, H. Kim, X.-M. Zhang, C.H. Dang, Y. Zhang, Y.J. Choi, A. Nurmikko, Z.L. Wang, *Nanotechnology* **21**, 095502 (2010)

Semiconductor Nanostructures for Optoelectronic
Devices

Processing, Characterization and Applications

Yi, G.-C. (Ed.)

2012, XIV, 338 p., Hardcover

ISBN: 978-3-642-22479-9